Design, Synthesis, and Cytotoxic Evaluation of a New Series of 3-Substituted Spiro[(dihydropyrazine-2,5-dione)-6,3′-(2′,3′-dihydrothieno[2,3-*b*]naphtho-4′,9′-dione)] Derivatives

Isabel Gomez-Monterrey,[†] Pietro Campiglia,[‡] Alfonso Carotenuto,[†] Daniela Califano,[§] Claudio Pisano,[||] Loredana Vesci,[||] Teresa Lama,[†] Alessia Bertamino,[†] Marina Sala,[†] Antonio Mazzella di Bosco,[†] Paolo Grieco,[†] and Ettore Novellino*[,†]

Dipartimento di Chimica Farmaceutica e Tossicologica, University of Naples "Federico II", Napoli, Dipartimento di Scienze Farmaceutica, Università di Salerno, Salerno I-84084, Fisciano, Oncologia Sperimentale E, Istituto dei Tumori Fondazione "G. Pascale", Napoli, and Area di Ricerca Oncologica—R&S, Sigma-Tau S.p.A., Pomezia, Roma, Italy

Received October 18, 2006

A series of 3-substituted spiro[(dihydropyrazine-2,5-dione)-6,3′-(2′,3′-dihydrothieno[2,3-*b*]naphtho-4′,9′-dione)] derivatives were prepared using an easy synthetic route via condensation of the 3-amino-3-(ethoxycarbonyl)-2,3-dihydrothieno[2,3-*b*]naphtho-4,9-dione system and amino acids followed by intramolecular lactamization. Amino acids containing alkyl and aryl, linear and cyclic, polar and apolar, and basic and acid residues were incorporated. Evaluation of these analogues against the MCF-7 human breast carcinoma and SW 620 human colon carcinoma cell lines revealed, for the 3*S*,3′*R* isomers derived from Pro (**7a**), Cys (**11a**), and Met (**12a**) and the 3*R*,3′*S* isomer derived from D-Pro (**7c**), a cytotoxic potency comparable to or greater than that of doxorubicin. Some of these selected analogues were potent cytotoxic agents in several other sensible and resistant human solid tumor cell lines and may be able to circumvent the multiple-drug-resistance mechanism. In particular, only a partial cross-resistance to the compounds **7**, **11**, and **12** was observed in selected tumor cell sublines known to be resistant to doxorubicin (MCF-7/Dx and A2780/Dx), whereas a very low level of cross-resistance to compounds **7** and **11** was found in a tumor cell subline selected for resistance to cisplatin (A2780/DDP). In addition, the topoisomerase II inhibition activity and DNA-binding properties were investigated.

Introduction

The antitumoral anthracyclines daunorubicin and doxorubicin and the synthetic anthracene-9,10-dione mitoxantrone are potent agents in clinical use today with broad application in the treatment of several leukemias and lymphomas as well as in combination chemotherapy of solid tumors.[1,2] The therapeutic relevance for these quinone derivatives has prompted intensive research into new structures with the goal of bypassing significant problems that limit the utility of these compounds, notably toxic dose-related side effects and development of drug resistance.[3−5] A large number of quinonic derivatives have been prepared, and several of these have shown promise in clinical studies.[6,7] Prominent examples are the azaanthracene derivative 6,9-bis[(2-aminomethyl)amino]benz[*g*]isoquinoline-5,10-dione dimaleate salt (BBR 2778),[8] the anthrapyrazole derivative losoxantrone (DuP-941)[9,10] (Figure 1), and some anthracenyl peptide derivatives which have been shown to be non-cross-resistant in MDR and AT-MDR cell lines and exhibited in vivo activity against tumor xenografts.[11,12] The mechanisms of cell-killing induction by these compounds are multimodal in nature. Their planarity allows an intercalation between specific base pairs of DNA, while their redox properties are linked to the production of radical species in biological systems.[13] The chemical and biological activity exhibited by these quinonic compounds is greatly affected by the different substituents of the planar ring system. The side chain usually bears one or two positive charges to establish an electrostatic interaction with the phosphate backbone of the polynucleotide. In addition, they meet the requirements for effective poisoning of topoisomerase II.[14−16] In fact, the mechanism of action appears to be mainly related to drug binding to the so-called "cleavable complex" formed by DNA and topoisomerase II.[17]

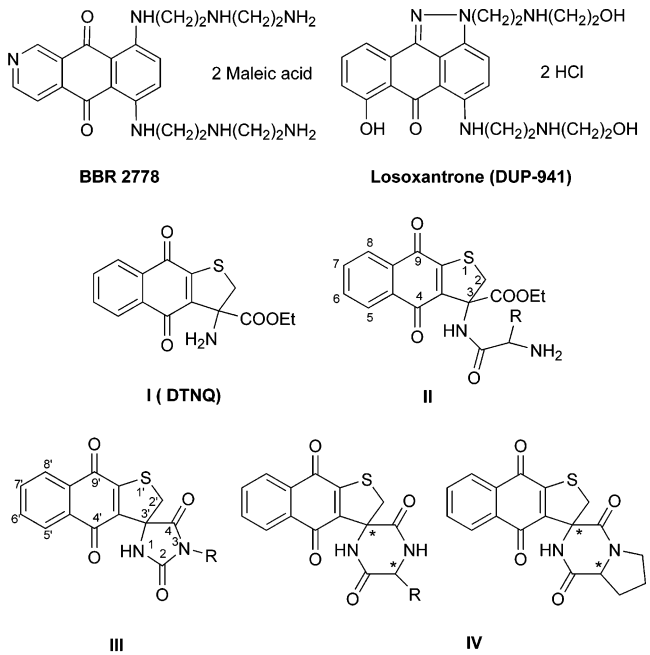

Figure 1. Structure of BBR 2778, losoxantrone, and the DTNQ template and its derivatives.

* To whom correspondence should be addressed. Phone: +39-081-678643. Fax: +39-081-678644. E-mail: novellin@unina.it.
[†] University of Naples "Federico II".
[‡] Università di Salerno.
[§] Istituto dei Tumori Fondazione "G. Pascale".
[||] Sigma-Tau S.p.A.

10.1021/jm0612158 CCC: $37.00
Published on Web 03/22/2007

Scheme 1[a]

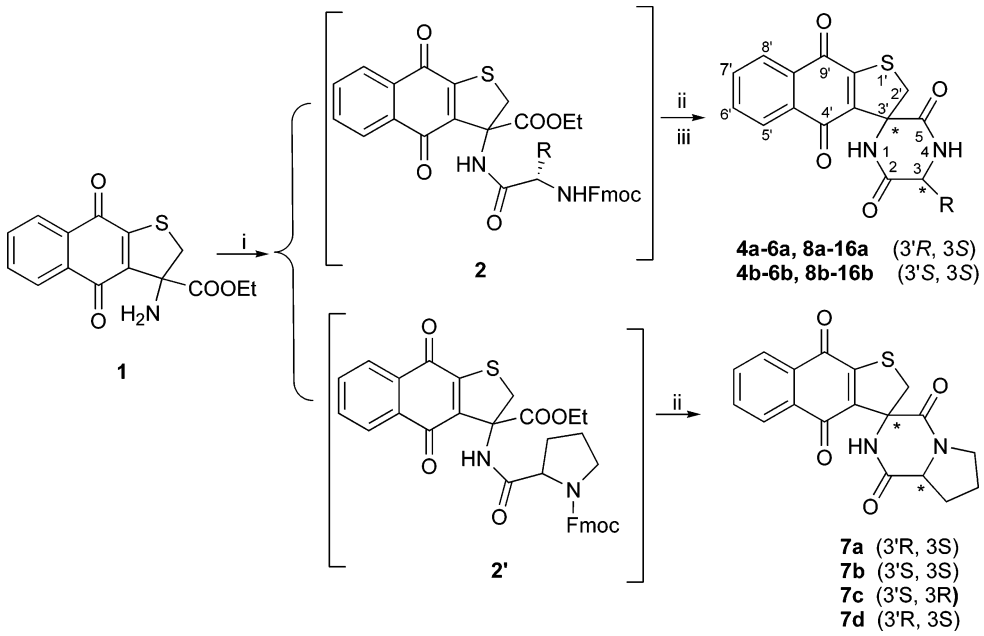

[a] Reagents and conditions: (i) Fmoc-Aa-OH, HBTU, HOBt, DMF, rt, 24 h; (ii) 20% piperidine/CH_2Cl_2, rt, 30 min, then MeOH, TEA, reflux, 1−3 h; (iii) 20% TFA in dichloromethane.

Therefore, the development of innovative agents and/or novel combinations is needed to improve the therapeutic effectiveness of this important class of compounds. In this regard, we have recently highlighted the potential value of a new planar ring system, the 3-amino-3-(ethoxycarbonyl)-2,3-dihydrothieno[2,3-*b*]naphtho-4,9-dione system (**I**, DTNQ), as a template in the development of effective cytotoxic agents (Figure 1).[18−20]

Previously, we explored the biological properties of two series related to the lead compound **I**. In the first series, we introduced amino acid and dipeptide residues in position 3 of the planar structure (general formula **II**).[19] The compound 3-(glycylamino)-3-(ethoxycarbonyl)-2,3-dihydrothieno[2,3-*b*]naphtho-4,9-dione (**2a,** R = H) retains cytotoxic activity at submicromolar concentration against several human leukemia and solid tumor cell lines. In the second series, we designed a set of spirohydantoin derivatives in which the planar chromophore (DTNQ) was combined, through the hydantoin ring, to different alkyl-, hydroxyalkyl-, and aminoalkyl-substituted side chains (general formula **III**). The 3-[2-(*N*,*N*-dimethylamino)ethyl or propyl]-spiro[(dihydroimidazo-2,4-dione)-5,3′-(2′,3′-dihydrothieno[2,3-*b*]naphtho-4′,9′-dione)] hydrochloride derivatives (**3a**, **3b**) showed remarkable biological activity, not only against several human solid tumor cell lines (comparable to that of doxorubicin), but also toward doxorubicin- and *cis*-platinum-resistant human cell lines.[20] The increment of cytotoxic activity observed for these DTNQ-based derivatives seems to indicate that the conformational restriction introduced by the hydantoin ring allows an optimal location of the planar ring relative to the side chain. On the basis of this finding, we decided to modify both the dimension and side-chain nature of the spiro nucleus attached to the DTNQ chromophore. Thus, a series of 3-substituted spiro-[(dihydropyrazine-2,5-dione)-6,3′-(2′,3′-dihydrothieno[2,3-*b*]-naphtho-4′,9′-dione)] derivatives as well as the pentacyclic analogues spiro[(hexahydropyrrolo[1,2-*a*]pyrazine-1,4-dione)-6,3′-(2′,3′-dihydrothieno[2,3-*b*]naphtho-4′,9′-dione)] were designed and synthesized (general formula **IV**). Our synthetic approach involves the condensation of the 3-amino-3-(ethoxycarbonyl)-2,3-dihydrothieno[2,3-*b*]naphtho-4,9-dione system with conveniently protected amino acids and subsequent intramolecular lactamization. This modification has been performed to define which functional side chain is critical for cytotoxic activity and to explore the structural parameters associated with the biological activity. Thus, Gly, Ala, Leu, L- and D-Pro, Phe, Tyr, Ser, Cys, Met, Lys, His, Asp, and Asn[a] were incorporated as suitable representatives for alkyl and aryl, linear and cyclic, polar and apolar, and basic and acid residues. The present paper deals with the synthesis, structural determination, and cytotoxic activity of this new series of compounds. In addition, some of the most active compounds were evaluated for their topoisomerase II inhibition activity and DNA-binding properties.

Results and Discussion

Chemistry. The preparation of the spirodiketopiperazine derivatives was performed following the synthetic route described in Scheme 1. The starting DTNQ was obtained by cycloaddition reaction between the 2-(4′-chlorophenyl)thiazolidine and naphthoquinone as we previously described.[18] The condensation of the DTNQ system with the corresponding *N*-Fmoc- and side-chain-protected amino acids, using HBTU and HOBt as condensating agents, afforded pseudodipeptide **2** or **2′** (from proline) as a mixture of diastereoisomers. Mildly acid-sensitive side-chain protecting groups (X = Boc, ^{t}Bu, Trt) were used for the synthesis of the derivatives containing Ser,

[a] Abbreviations: AAA, amino acid analysis; Boc, *tert*-butyloxycarbonyl; Trt, trityl; ^{t}Bu, *tert*-butyl; CH_3CN, acetonitrile; DCM, dichoromethane; DIPEA, *N*,*N*-diisopropylethylamine; DMF, *N*,*N*-dimethylformamide; DQF-COSY, double-quantum-filtered correlated spectroscopy; Et_3SiH, triethylsilane; FAB-MS, fast-atom bombardment mass spectrometry; Fmoc, 9-fluorenylmethoxycarbonyl; HOBt, *N*-hydroxybenzotriazole; HBTU, 2-(1*H*-benzotriazol-1-yl)-1,1,3,3-tetramethyluronium hexafluorophosphate; MD, molecular dynamic; NOE, nuclear Overhauser effect; NOESY, nuclear Overhauser enhancement spectroscopy; Pbf, 2,2,4,6,7-pentamethyldihydrobenzofuran-5-sulfonyl; FC, flash chromatography; RP-HPLC, reversed-phase high-performance liquid chromatography; SDS, sodium dodecyl sulfate; TFA, trifluoroacetic acid; TLC, thin-layer chromatography; TOCSY, total correlated spectroscopy; Trt, triphenylmethyl (trityl). Abbreviations used for amino acids and designation of peptides follow the rules of the IUPAC-IUB Commission of Biochemical Nomenclature in *J. Biol. Chem.* **1972**, *247*, 977−983. Amino acid symbols denote the L-configuration unless indicated otherwise.

Table 1. Cytotoxic Activity of 3-Substituted Spiro[(dihydropirazine-2,5-dione)-6,3′-(2′,3′-dihydrothieno[2,3-*b*]naphtho-4′,9′-dione)] Derivatives **4a,b**−**6a,b** and **8a,b**−**16a,b** and Spiro[(hexahydropyrrolo[1,2-*a*]pyrazine-1,4-dione)-6,3′-(2′,3′-dihydrothieno[2,3-*b*]naphtho-4′,9′-dione)] Derivatives **7a**−**c**

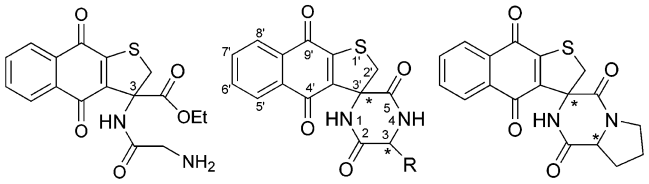

			IC_{50}[a] (μM ± SD)	
compd	stereochemistry 3,3′	R	MCF-7[b]	SW620[c]
2a	3*SR*	H	0.196 ± 0.005	1.100 ± 0.001
4a,b	3′*SR*	H	0.047 ± 0.001	0.245 ± 0.036
4a	3′*R*	H	0.046 ± 0.001	0.267 ± 0.008
4b	3′*S*	H	0.049 ± 0.001	0.326 ± 0.010
5a	3*S*,3′*R*	CH_3	0.053 ± 0.013	0.287 ± 0.014
5b	3*S*,3′*S*	CH_3	0.098 ± 0.010	0.776 ± 0.014
6a	3*S*,3′*R*	$CH_2CH(CH_3)_2$	0.090 ± 0.013	0.414 ± 0.030
6b	3*S*,3′*S*	$CH_2CH(CH_3)_2$	0.160 ± 0.007	0.476 ± 0.011
7a	3*S*,3′*R*	cyclo($CH_2CH_2CH_2$)−	0.020 ± 0.004	0.120 ± 0.030
7b	3*S*,3′*S*	cyclo($CH_2CH_2CH_2$)−	0.263 ± 0.047	0.840 ± 0.030
7c	3*R*,3′*S*	cyclo($CH_2CH_2CH_2$)−	0.017 ± 0.008	0.010 ± 0.020
7d	3*R*,3′*R*	cyclo($CH_2CH_2CH_2$)−	0.213 ± 0.060	1.200 ± 0.300
8a	3*S*,3′*R*	$CH_2C_6H_5$	0.060 ± 0.010	0.445 ± 0.170
8b	3*S*,3′*S*	$CH_2C_6H_5$	0.140 ± 0.040	0.459 ± 0.180
9a	3*S*,3′*R*	$CH_2C_6H_4$(4-OH)	0.085 ± 0.009	0.700 ± 0.050
9b	3*S*,3′*S*	$CH_2C_6H_4$(4-OH)	0.154 ± 0.010	1.000 ± 0.300
10a	3*S*,3′*R*	CH_2OH	0.243 ± 0.030	0.894 ± 0.040
10b	3*S*,3′*S*	CH_2OH	0.456 ± 0.050	1.530 ± 0.250
11a	3*R*,3′*R*	CH_2SH	0.029 ± 0.009	0.210 ± 0.008
11b	3*R*,3′*S*	CH_2SH	0.069 ± 0.009	0.224 ± 0.050
12a	3*S*,3′*R*	$CH_2CH_2SCH_3$	0.036 ± 0.009	0.229 ± 0.031
12b	3*S*,3′*S*	$CH_2CH_2SCH_3$	0.108 ± 0.019	0.765 ± 0.100
13a[d]	3*S*,3′*R*	$(CH_2)_4NH_2$	0.083 ± 0.011	0.825 ± 0.079
13b[d]	3*S*,3′*S*	$(CH_2)_4NH_2$	0.179 ± 0.007	1.715 ± 0.160
14a	3*S*,3′*R*	CH_2-imidazole	0.660 ± 0.111	1.929 ± 0.163
14b	3*S*,3′*S*	CH_2-imidazole	1.850 ± 0.102	>4000
15a	3*S*,3′*R*	CH_2COOH	1.700 ± 0.110	0.285 ± 0.059
15b	3*S*,3′*S*	CH_2COOH	1.930 ± 0.050	>4000
16a	3*S*,3′*R*	CH_2CONH_2	0.351 ± 0.030	1.528 ± 0.032
16b	3*S*,3′*S*	CH_2CONH_2	0.835 ± 0.013	3.353 ± 0.079
doxorubicin			0.022 ± 0.008	0.178 ± 0.003

[a] Data represent mean values (±SD) for three independent determinations. [b] Human breast carcinoma cell line. [c] Human colon carcinoma cell line. [d] Evaluated as TFA salts.

Cys, Lys, Hys, Asp, and Asn. Then, Fmoc-amino deprotection in 20% piperidine/CH_2Cl_2 and successive treatment with TEA in MeOH at reflux afforded the corresponding 3-substituted spiro[(dihydropyrazine-2,5-dione)-6,3′-(2′,3′-dihydrothieno[2,3-*b*]naphtho-4′,9′-dione)] derivatives **4**−**6**, **8**, and **12** and the spiro-[(hexahydropyrrolo[1,2-*a*]pyrazine-1,4-dione)-6,3′-(2′,3′-dihydrothieno[2,3-*b*]naphtho-4′,9′-dione)] derivatives **7** in 46−60% overall yields.

Finally, after removal of the side-chain protecting group using 20% TFA in dichloromethane, the final compounds **9**−**11** and **13**−**16** were obtained in 36−53% overall yields. Since the synthetic pathway used for the preparation of the starting DTNQ generates an asymmetric carbon (C-3) in this system, the final compound **4** (derived from Gly) was obtained as a racemic mixture, while the other compounds were obtained as diastereoisomer mixtures. The synthesis of the enantiomerically pure compounds **4a** and **4b** was performed starting from Fmoc-Gly and pure enantiomers of DTNQ, which were resolved according to the procedure previously described.[18,21] For the other compounds (**5**−**16**), HPLC analysis of the resulting crude products showed the presence of both 3*S*,3′*R* (**a**) and 3*S*,3′*S* (**b**) diastereoisomers (**a**/**b** = 3/2 to 1/1 ratio), which in all cases were separated after flash chromatography. The same procedure allowed the separation of **7c** (3*R*,3′*S*) and **7d** (3*R*,3′*R*) obtained from D-Pro. The physicochemical properties and purity of the final compounds were assessed by TLC, LC−MS, analytical RP-HPLC, and NMR analysis (Experimental Section).

Stereochemistry Determination. The determination of the absolute configuration at the C-3′ asymmetric center was performed by an NMR study of representative derivatives **7a**, **7b**, **8a**, **8b**, **9a**, **9b**, **14a**, and **14b**, which showed a major descrimination by NMR. The only difference observed in the 2D NOESY[22] spectra of "type **a**" derivatives compared to "type **b**" (Supporting Information) was the presence in the last of NOE contacts of both H-2′^{a} (H-2′ low-field signal) and H-2′^{b} (H-2′ high-field signal) with H-3 (corresponding to Hα of the proline moiety). Inspections of molecular models obtained by molecular dynamic simulation (Experimental Section) showed that the distances of both H-2′(s) and H-3 were about 3.9 Å in the 3*S*,3′*S* isomer and about 5.2 Å in the 3*S*,3′*R* isomer. Hence, the stereochemistry 3*S*,3′*R* could be assigned to compounds of type **a** and 3*S*,3′*S* to compounds of type **b**. The above assignment is in accordance with the downfield shift observed for the H-2′^{a} signal in compounds **a** compared to the same signal in

Table 2. Inhibition of Multiple Human Tumor Cell Lines by Selected Compounds

	IC_{50}[a] (μM ± SD)					
compd	A2780ovarian	NCI-H460 lung	HCT-116 ilocecal	PC-3 prostate	LoVo colon	MeVo melanoma
7a	0.105 ± 0.001	0.114 ± 0.01	0.090 ± 0.010	0.153 ± 0.01	0.420 ± 0.03	0.075 ± 0.01
7b	0.530 ± 0.03	0.994 ± 0.10	0.838 ± 0.030	0.610 ± 0.09	1.410 ± 0.10	0.570 ± 0.004
7c	0.036 ± 0.002	0.052 ± 0.01	0.240 ± 0.002	0.110 ± 0.01	0.320 ± 0.06	0.150 ± 0.01
7d	0.190 ± 0.02	0.170 ± 0.01	3.300 ± 0.100	1.900 ± 0.30	1.700 ± 0.02	7.200 ± 1.60
11a	0.190 ± 0.02	0.470 ± 0.04	0.350 ± 0.030	0.307 ± 0.05	0.870 ± 0.10	0.075 ± 0.02
11b	0.460 ± 0.15	0.730 ± 0.06	0.660 ± 0.020	0.367 ± 0.058	1.300 ± 0.10	0.567 ± 0.10
12a	0.180 ± 0.03	0.256 ± 0.03	0.256 ± 0.010	0.293 ± 0.017	0.540 ± 0.07	0.057 ± 0.01
12b	0.624 ± 0.05	0.917 ± 0.03	0.766 ± 0.050	0.582 ± 0.05	0.620 ± 0.05	1.130 ± 0.05
doxorubicin	0.007 ± 0.001	0.010 ± 0.008			0.033 ± 0.004	0.820 ± 0.10

[a] Data represent mean values (±SD) for three independent determinations.

compounds **b**, which, actually, represents the most significant resonance difference between **a** and **b** ^{1}H NMR spectra. Molecular models showed that the distance between H-2′[a] and carbonyl oxygen O-5 is smaller in compounds **a** compared to compounds **b** (2.5−2.7 Å vs 2.8−3.0 Å). It can be hypothesized that the resulting deshielding of H-2′[a] explains the observed resonance shift. Once the stereochemistry of C-3′ in stereoisomer couples **7**, **8**, **9**, and **14** was assigned, we acquired the CD spectra of these compounds. We expected a significant difference in their CD spectra due to the inversion of the chiral center C-3′. In fact, the inversion of a chiral center in the immediate vicinity of a chromophore group is also expected to invert the sign of the Cotton effects of the relevant absorption band(s).[23] Actually, the CD spectrum of compounds **7a**, **8a**, **9a**, and **14a** (3*S*,3′*R*) showed a negative Cotton effect centered around 320 nm and a positive Cotton effect around 290 nm, while compounds **7b**, **8b**, **9b**, and **14b** (3*S*,3′*S*) showed inverted Cotton effects at the same wavelengths (Supporting Information). Starting from these results, we were able to assign the absolute stereochemistry of the other **a**/**b** diastereisomer couples on the basis of their CD spectra (Supporting Information). Interestingly, in all diastereisomer couples, a downfield shift of the H-2′[a] signal confirmed the assignment of the relevant compound to the 3*S*,3′*R* series. Finally, the stereochemistries of compounds **7c** and **7d** were easily discriminated by NMR and CD analysis considering their enantiomeric relationship with compounds **7a** and **7b**, respectively.

In Vitro Cytotoxicity. Preliminarily, the cytotoxic activity of all diketopiperazine derivatives was evaluated toward the MCF-7 human breast carcinoma and SW 620 human colon carcinoma cell lines (Table 1). For comparative purposes, doxorubicin and the linear pseudodipeptide analogue **2a** were also included in the assay. As shown in Table 1, compound **4** in racemically and enantiomerically pure forms showed a potent cytotoxic activity on the MCF-7 and SW 620 cell lines, being about 4-fold more active with respect to compound **2a** and only 2-fold less potent than doxorubicin.

The improved antitumor activity and spectra of these newly synthesized compounds, compared to the linear **2a**, demonstrated that C3′ chemical modification was indeed an effective approach to optimize the activity profiles of DTNQ derivatives.[19]

The results in Table 1 reveal some important structure−activity relationships. First, the wide activity range observed for compounds **5**−**16** (IC_{50} = 17−1930 nM, on the MCF-7 cell line) indicated that the nature of the substituents on C-3 of the diketopiperazine moiety markedly affects the activity profile of these compounds. Second, the relative configurations at the 3 and 3′ carbons have an important influence on the cytotoxic activity of these compounds, defining a preferential positioning of the side-chain substituents. Thus, the 3*S*,3′*R* and 3*R*,3′*S* diastereoisomers were, in general, 2- or 3-fold more potent than the corresponding 3*S*,3′*S* and 3*R*,3′*R* diastereoisomers. The incorporation at position 3 of a small alkyl substituent (CH_3, **5a**) was well tolerated, but a marginal loss in activity was obtained with compound **6** (2-fold) by increasing the steric bulk of the alkyl side chain. A further conformational restriction introduced by the L- and D-Pro amino acids gave the most interesting and potent derivatives of this series. In fact, **7a** and its enantiomer **7c** (IC_{50} = 20 and 17 nM, respectively) were 10-fold more potent than the corresponding diasteroisomers **7b** and **7d** and showed an activity similar to that of doxorubicin on the MCF-7 cell line. In addition, compound **7c** was 17-fold more active than doxorubicin on the SW 620 cell line (IC_{50} = 10 vs 178 nM).

The presence of a benzyl group (**8a,b**), relatively rigid and more electron rich when compared to the alkycyclic proline side chain, led to significant loss of activity (3-fold). Replacement of a hydroxybenzyl group (**9a,b**) instead of a benzyl group further decreased the cytotoxic activity. The incorporation of amino acids containing sulfur gave the potent derivatives **11a** and **12a**, which retained a cytotoxic level similar to that of compounds **7a** and **7c** and doxorubicin (IC_{50} = 29 and 36 nM, respectively). The compounds containing hydroxyl (**10a),** amino (**13a**), or imidazole (**14a)** groups in the side chain were respectively 12-, 4-, and 33-fold less potent than compound **7a**. Overall, these data suggest that a hydrophobic interaction might exist between the target and this molecular area of the drugs. Finally, the presence of a free carboxyl function in **15** led to a dramatic reduction in cell growth inhibition of these cell lines. This observation would indicate that the diketopiperazine molecular area might interact with the DNA minor groove, and thereby, a negative charge in this area would be disfavored. In fact, the amide analogue **16a** was 5-fold more potent than **15a**.

To further determine their antitumor spectra and drug-resistance profile, compounds **7**, **11**, and **12** were selected and screened against a panel of human tumor cell lines (Table 2), including selected breast and ovarian cellular sublines resistant to doxorubicin (MCF-7/Dx and A2780/Dx) and resistant to cisplatin (A2780/DDP) (Table 3). As observed in the case of the MCF-7 and SW620 cell lines, the diastereoisomers with configuration 3*S*,3′*R* (**7a**, **11a**, **12a**) or 3*R*,3′*S* (**7c**) were the most potent derivatives. In the tested A2780 (ovarian), NCI-H460 (lung), HCT-116 (ilocecal), and PC-3 (prostate) cell systems, compounds **7a** and **7c** showed marked cytotoxic potency (Table 2) and were less active against LoVo (colon) tumor cells (IC_{50} = 420 and 320 nM, respectively). Interestingly, compounds **7a**, **11a**, and **12a** were 11-, 11-, and 14-fold more potent than doxorubicin in MeVo (melanoma) tumor cells (IC_{50} = 75, 75, and 57 nM).

Table 3. Inhibition of Drug-Resistant Tumor Cell Lines by Selected Compounds

	IC_{50}[a] (μM ± SD)							
compd	MCF-7 breast	MCF-7/Dx[b] breast	RI[c]	A2780 ovarian	A2780/Dx[b] ovarian	RI[c]	A2780/DDP[d] ovarian	RI[c]
7a	0.020 ± 0.004	0.074 ± 0.03	3.7	0.105 ± 0.001	0.160 ± 0.02	1.5	0.256 ± 0.03	2.4
7b	0.263 ± 0.047	0.340 ± 0.03	1.3	0.530 ± 0.03	0.760 ± 0.07	1.4	0.793 ± 0.01	1.5
7c	0.017 ± 0.008	0.041 ± 0.020	2.4	0.036 ± 0.002	0.150 ± 0.01	5.8	0.420 ± 0.01	10
7d	0.213 ± 0.060	0.234 ± 0.10	1.1	0.190 ± 0.02	3.200 ± 0.10	4.2	5.500 ± 0.09	11.7
11a	0.029 ± 0.009	0.032 ± 0.01	1.1	0.190 ± 0.02	1.200 ± 0.30	6.3	1.890 ± 0.30	10
11b	0.069 ± 0.009	0.193 ± 0.02	2.8	0.460 ± 0.15	0.980 ± 0.20	2.1	1.130 ± 0.10	2.4
12a	0.036 ± 0.009	0.158 ± 0.03	4.4	0.180 ± 0.03	0.450 ± 0.05	2.5	0.789 ± 0.02	4.4
12b	0.108 ± 0.019	0.302 ± 0.02	2.8	0.624 ± 0.05	1.560 ± 0.20	2.5	3.359 ± 0.02	4.4
doxorubicin	0.022 ± 0.008	5.300 ± 0.40	286	0.007 ± 0.001	0.290 ± 0.01	41	0.007 ± 0.001	1[e]

[a] Data represent mean values (±SD) for three independent determinations. [b] Subline resistant to doxorubicin. [c] Resistance index: ratio between the IC_{50} of resistant and sensitive tumor cell lines. [d] Subline resistant to cisplatin. [e] The RI for cisplatin on A2780/ DDP was 28.

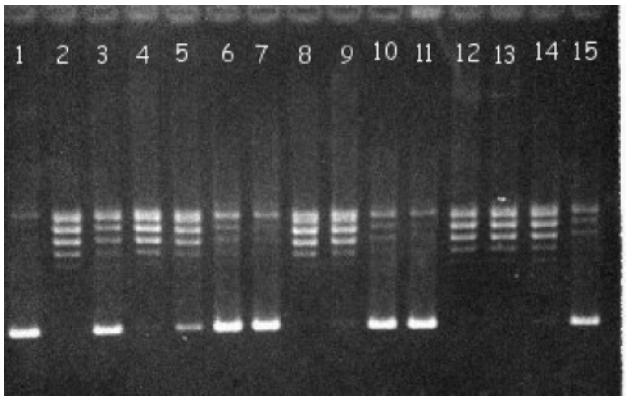

Figure 2. Effects of compounds **5a**, **6a**, and **7b** on the DNA-relaxing activity of human top2: lane 1, pBR322 DNA; lane 2, pBR322 + top2; lane 3, pBR322 + top2 + VP-16, 25 μM; lanes 4, 5, 6, and 7, pBR322 + top2 + **5a** (1, 5, 10, and 25 μM, respectively); lanes 8, 9, 10, and 11, pBR322 + top2 + **6a** (1, 5, 10, and 25 μM, respectively); lanes 12, 13, 14, and 15, pBR322 + top2 + **7b** (1, 5, 10, and 25 μM, respectively).

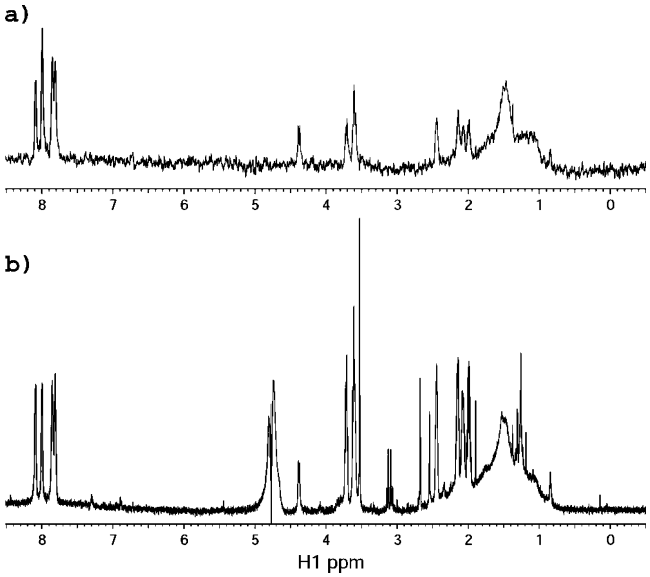

Figure 3. (a) STD NMR spectrum of the **7a** (1 mM)/DNA (50 μM) complex recorded upon saturation at −1 ppm. (b) Corresponding 1D proton spectrum.

When tested against multiple resistance tumor cells (Table 3), these compounds retained good inhibition against selected breast and ovarian cellular subclones resistant to both doxorubicin (MCF-7/Dx and A2780/Dx) and cisplatin (A2780/DDP). In particular, the MCF-7/Dx cell line exhibited a low level of cross-resistance to all derivatives **7**, **11**, and **12** (RI (resistance index) = 1.1−4.4), whereas a very low cross-resistance to **7a, 7b**, **11b**, **12a**, and **12b** was observed in the ovarian doxorubicin-resistant subline A-2780/Dx (RI = 1.4−2.5). Moreover, the cisplatin-resistant ovarian subclone (A2780/DDP) showed low levels of cross-resistance to compounds **7a**, **7b**, and **11b** (RI = 2.4, 1.5, and 2.4, respectively).

Drug Inhibition of DNA Relaxation Induced by Topoisomerase II (top2). The relative drug activity in inhibiting top2-mediated DNA relaxation was studied using supercoiled pBR322 DNA as a substrate for human top2 and etoposide (VP-16) as a top2-specific inhibitor.[24] The preliminary experiments indicated that the compounds containing linear and cyclic alkyl side chains (**5a**, **6a**, and **7b**) exhibited potent inhibitory activity at a concentration of 10 μM **(**Figure 2). The most potent cytotoxic compounds **7a**, **7c**, **11a**, and **12a** inhibited top2 catalytic activity in the concentration range 25−50 μM (data not shown), whereas the remaining compounds did not inhibit top2 catalytic activity at a concentration of 50 μM.

These results demonstrate that there is not an exact correlation between cytotoxicity in cancer cell cultures and top2 inhibitory activity. Differences in cellular uptake, distribution within the cell, and additional targets within the cell may all play a role, thus making the correlation of cytotoxicity with top2 inhibitory activity less than perfect. A similar finding was reported previously with 9-substituted acridine derivatives, acridine polyamine conjugates, and indenoisoquinolines and topoisomerase I or II inhibition.[25−27]

DNA Binding Properties. Saturation Transfer Difference (STD) NMR. Compound **7a** was tested to see whether it interacts with DNA using the STD-NMR[28,29] technique. STD-NMR is a technique that can be used to characterize and identify binding. This technique has become increasingly important as a tool in the investigation of biomolecular recognition phenomena. The STD-NMR technique is a method of epitope mapping and ligand screening by NMR spectroscopy. Resonances of the macromolecule are selectively saturated, and in a binding ligand, enhancements are observed in the difference (STD-NMR) spectrum arising from subtraction of this spectrum from a reference spectrum in which the macromolecule is not saturated. Protons of the ligand which are in close contact with the macromolecule can easily be identified from the STD-NMR spectrum, because they are saturated to the highest degree. They should have a stronger STD, and this allows direct observation of areas of the ligand that comprises the epitope. We investigated the interaction of compound **7a** with calf thymus DNA. The 1D ^{1}H NMR and STD-NMR spectra of **7a** in the presence of calf thymus DNA are shown in Figure 3. The 1D ^{1}H NMR spectrum of **7a** in the presence of calf thymus DNA (Figure 3b) displayed broad signals around 3.0−0.8 ppm, normal for long-chain DNA, and sharp resonance signals at 3.52, 3.11, 2.55,

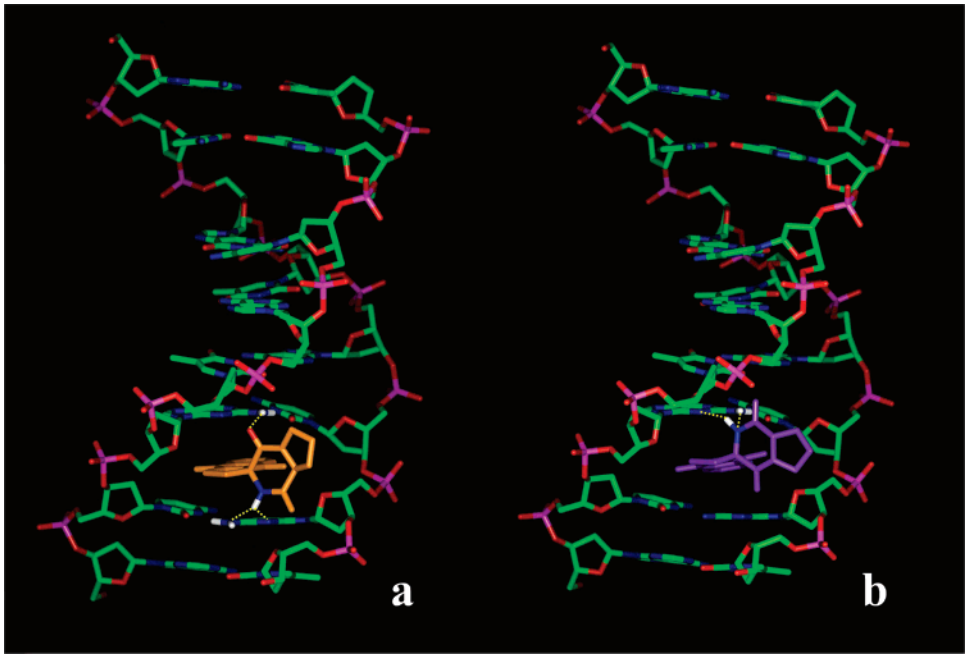

Figure 4. A side view of the energy-minimized average structure from the 70 ps period of the MD simulation of complexes (a) **7a**/[d(ACGTACGT)]$_2$ and (b) **7b**/[d(ACGTACGT)]$_2$.

and 1.90 and around 1.3 ppm arising from low molecular weight molecules of the buffer solution (EDTA, Tris) and impurities. These latter peaks were not present in the corresponding STD spectrum because these molecules do not bind to the DNA (Figure 3a). In contrast, all the proton resonances of **7a** were observed in the STD spectrum, demonstrating that **7a**/DNA interactions did occur.

Di Micco et al. have recently devised an elegant STD-based method, named DF-STD (differential frequency STD) spectroscopy,[30] that allows the study of small-molecule−DNA binding modes. In particular, the method allows the discrimination of base-pair intercalators and minor-groove and external binders. The approach is based on the comparison of two parallel sets of STD experiments performed under the same experimental conditions, in which saturation is centered either in the aromatic or in the low-field aliphatic spectral regions. Due to the anisotropy in the efficiency of saturation diffusion along the vertical and horizontal dimensions of helical DNA, a ligand making proximate contacts with aromatic base protons, such as an intercalator sandwiched by consecutive base pairs, would receive more saturation upon irradiation of DNA aromatic protons rather than irradiation of deoxyribose protons. Conversely, an external ligand presenting the majority of its binding surface in contact with the DNA phosphodiester backbone should be more affected by irradiation in the deoxyribose region rather than by irradiation in the DNA aromatic region. To facilitate analysis of the DF-STD data, the authors introduced the "binding mode index" (BMI), a numerical parameter that expresses the relative sensitivity of ligand protons to the perturbation arising from each type of saturation (that is, base versus sugar/backbone saturation). Three BMI ranges could be extrapolated: $0 < \text{BMI} < 0.50$ for external (nonspecific) electrostatic backbone binding, $0.90 < \text{BMI} < 1.10$ for minor-groove binding, and $1.20\ (0.90) < \text{BMI} < 1.50$ for base-pair intercalation. DF-STD analysis of compound **7a** was performed using the poly(dG-dC)·poly(dG-dC) copolymer as the DNA target since the absence of the thymine methyl groups allows a selective irradiation of the aliphatic (0.5 ppm) or aromatic (9.00 ppm) regions. Two different BMI values were obtained: BMI = 1.38 for the quasi-planar tricyclic portion and BMI = 0.28 for the proline portion. This result can be explained assuming two different DNA binding modes for **7a**. An intercalative mode of binding is sustained by its tricyclic planar core, and an external backbone binding can be attributed to its proline moiety. Interestingly, the DF-STD finding for **7a** is very similar to that observed for doxorubicin (BMI = 1.33 for the intercalating tricyclic chromophoric core and BMI = 0.20 for the amino sugar moiety).[30] We performed the same analysis on compound **16a**, which bears a more flexible side chain compared to compound **7a** and which shows an intermediate cytotoxic activity in this series. A DF-STD profile similar to that of **7a** was observed for **16a**, indicating an analogous binding mode for these compounds.

Model Building and MD Simulation of the 7a,b/DNA Complexes. Models of a DNA octamer complexed to compounds **7a** and **7b** were built by automatic docking (AutoDock) and extensive energy minimization and equilibration[31] on the basis of the NMR structure of a bisdaunorubicin (WP631) bound to [d(ACGTACGT)]$_2$ (see the Experimental Section for details).[32]

From the AutoDock result, the DTNQ chromophore of **7a** binds at the middle 5′-GC-3′ base pairs of double-stranded DNA by intercalation, whereas diketopiperazine and proline rings are placed externally (Figure 4a). Starting from the best scored conformation of the complex **7a**/DNA given by AutoDock, a free MD trajectory (70 ps) was generated at 300 K using the Discover module present in InsightII (Accelrys, San Diego, CA). The trajectory was sampled every 1 ps and examined visually by using the InsightII program. Inspection of the MD trajectory, during which the drug remains inserted in the DNA and fully intercalating at the 5′-GC-3′ steps, led to the following observations: Watson−Crick base−base hydrogen bond distances are conserved during the simulation with an average value around 2 Å; an average Watson−Crick base−base distance C1′−C1′ and base−base angle N1−C1′−C1′ for pyrimidines or N9−C1′−C1′ for purines are 10.9 Å and 64.4° with root-mean-square deviations (rmsd's) of 0.3 Å and 9°, respectively, in agreement with standard values for B-DNA (10.85 Å and 51.5°).[33] After

the initial heating to 300 K, the rmsd profile, calculated for all atoms from the initial energy-minimized complex, remains stable for the rest of the simulation (1.8 ± 0.3 Å), indicating that the drug/DNA complex settles into a well-defined and stable configuration during the simulation. As shown in Figure 4a, the complex **7a**/[d(ACGTACGT)]$_2$ is stabilized by hydrogen bonds and by $\pi-\pi$ stacking forces. The amide N1 hydrogen of **7a** forms hydrogen bonds with N2 and N3 atoms of the guanidine G15 at the intercalation site. Furthermore, one of the amine hydrogens on N2 of guanine G3 forms another hydrogen bond with O5 of the diketopiperazine ring of **7a**. These hydrogen-bonding interactions were present in the initial model and were maintained for the whole length of the monitored simulation period.

The model reported in Figure 4a suggests that the intercalation of **7a** with DNA also involves $\pi-\pi$ stacking interactions of the quinone moiety with the five- and six-membered rings of the overlying guanine G15 and of the underlying guanine G3. Finally, favorable van der Waals contacts are observable between the proline Cβ methylene and the C4′ methine group of the deoxyribose ring of the guanine G15 residue. This model fully agrees with the experimental STD-NMR results.

For compound **7b**, we obtained very similar results in the simulation study (Figure 4b). The most important difference observed in the **7b**/DNA complex compared to the **7a**/DNA complex was the absence, in the first, of the hydrogen bonds between the N1 hydrogen of the drug with N2 and N3 atoms of the guanidine G3. Accordingly, the rmsd profile of the **7b**/DNA complex (calculated for all atoms from the initial energy-minimized complex) during the MD simulation increased to 4.2 ± 0.3 Å, indicating that it was less stable than the **7a**/DNA complex. The different stabilities of these complexes can explain the reduction in cytotoxic potency (about 10-fold) of **7b** compared to **7a** observed for almost all the tested cell lines (see above).

Conclusions

We report here the synthesis and biological evaluation of new spirodiketopiperazine derivatives of the dihydrothieno[2,3-*b*]-naphtho-4,9-dione system which exhibit activity against different tumor cell lines. Most active compounds **7a**,**c**, **11a**, and **12a** showed similar or improved activities compared to doxorubicin on the MCF-7 and SW620 cell lines. The ability of these compounds to overcome potential multiple-drug-resistance mechanisms has also been demonstrated by their cytotoxicity on doxorubicin- and cisplatin-resistant cell lines. STD-NMR spectroscopy investigation performed on compounds **7a** and **16a** demonstrated that they interact with DNA with a dual binding mode: intercalative for the tricyclic planar core and external considering the side-chain moiety. A three-dimensional structural model was developed in which compounds **7a** and **7b** intercalate at the middle 5′-GC-3′ base pairs of double-stranded DNA. The complexes are stabilized by $\pi-\pi$ stacking interactions, by a proposed set of hydrogen bonds, and by van der Waals contacts. This proposed interaction model might explain the high cytotoxicity of the active compounds. Other factors such as differences in cellular uptake, distribution within the cell, and/or an additional target within the cell might also affect the cytotoxicity of these derivatives.

Experimental Section

General Procedures. Reagents, starting material, and solvents were purchased from commercial suppliers and used as received. Analytical TLC was performed on a 0.25 mm layer of silica gel 60 F_{254} (Merck) and preparative TLC on 20 × 20 cm glass plates coated with a 2 mm layer of silica gel PF_{254} (Merck). Silica gel 60 (300−400 mesh, Merck) was used for flash chromatography. Melting points were taken on a Kofler apparatus and are uncorrected. Optical rotations were determined with a Perkin-Elmer-241 MC polarimeter. Mass spectra were obtained using an FAB-MS spectrometer. Analytical RPHPLC was performed on a Vydac C-18 (25 × 0.46 cm) columm, using a tunable UV detector set at 215 nm. Elution was performed with a linear gradient from 10% to 60% acetonitrile in 0.1% aqueous TFA over 55 min at a flow rate of 1 mL/min. The DTNQ system was synthesized according to the procedure previously described,[20] using ethyl 2-(4-chlorophenyl)-1,3-thiazolidine-4-carboxylate and naphthoquinone as starting material. The enantiomerically pure (+)- and (−)-DTNQ were synthesized according to the procedure previously described.[20,21]

General Procedure for the Synthesis of 3-Substituted Spiro-[(dihydropyrazine-2,5-dione)-6,3′-(2′,3′-dihydrothieno[2,3-*b*]-naphtho-4′,9′-dione)] Derivatives 4−6 and 8−16 and Spiro-[(hexahydropyrrolo[1,2-*a*]pyrazine-1,4-dione)-6,3′-(2′,3′-dihydrothieno[2,3-*b*]naphtho-4′,9′-dione)] Derivatives 7. To a solution of DTNQ (1−2 mmol) in dichloromethane/DMF (20 mL/5 mL) were successively added the corresponding *N*-Fmoc-protected amino acid Gly, Ala, Leu, Pro, D-Pro, Phe, Tyr(^{t}Bu), Ser(^{t}Bu), Cys-(Trt), Met, Lys(Boc), Hys(Trt), Asp(^{t}Bu), or Asn(Trt) (1.1 equiv), HBTU (1.2 equiv), HOBt (1.2 equiv), and DIEA (2.4 equiv), and stirring was continued at room temperature for 48 h. Afterward, the reaction mixture was diluted with dichloromethane (20 mL), and the resulting solution was washed successively with 10% citric acid (2 × 25 mL), 10% $NaHCO_3$ (2 × 25 mL), and water (2 × 25 mL), dried over Na_2SO_4, and evaporated to dryness. The residue was dissolved in CH_2Cl_2 (5 mL), and a solution of 20% piperidine in DMF (5−10 mL) was added. Stirring was continued for 30 min at room temperature and for 2 h at reflux temperature. The reaction mixture was allowed to warm to room temperature and evaporated to dryness. Flash chromatography of the residues, using different eluent systems, yielded, in each case, the correspondent final spirodiketopiprerazine derivatives **4**−**8** and **12** and the side-chain-protected derivatives **9′**−**11′** and **13′**−**16′**.

General Procedure for Removal of the Side-Chain Protecting Groups. A solution of side-chain-protected derivatives **9′**−**11′** and **13′**−**16′** (0.03−0.05 mM) in dichloromethane (10 mL) was treated with trifluoroacetic acid (2 mL) and stirred at room temperature for 1−3 h. After evaporation to dryness, the treatment of the residue with dichloromethane and diethyl ether yielded the corresponding final compounds **9**−**11** and **13**−**16.** The purity of all these compounds was assessed as being >98% using HPLC, microanalyses, and NMR spectroscopy.

Data for spiro[(dihydropyrazine-2,5-dione)-6,3′-(2′,3′-dihydrothieno[2,3-*b*]naphtho-4′,9′-dione)] (4): FC in 10% MeOH in $CHCl_3$; yellow solid (51%); mp 197−201 °C; HPLC t_R 17.92 min; ^{1}H NMR (500 MHz, CD_3OD) δ 3.55 (d, 1H, J = 12.9 Hz, H-2′^{b}), 4.06 (d, 1H, J = 16.2 Hz, H-3) 4.21 (d, 1H, H-2′^{a}), 4.27 (d, 1H, H-3′), 7.69−7.76 (m, 2H, H-6′ and H-7′), 8.03 (d, 1H, J = 7.1 Hz, H-5′ or H-8′), 8.07 (d, 1H, H-8′ or H-5′); FAB-MS *m*/*z* calcd for $C_{15}H_{10}N_2O_4S$ 314.32, found 314.51. The pure enantiomers (3′*R*)-**4a** and (3′*S*)-**4b** were prepared from the corresponding (+)- and (−)-DTNQ and glycine following the general procedure indicated above. Data for **4a**: $[\alpha]_D^{20}$ = −24.8° (*c* 1.0, MeOH); mp 196−198 °C. Data for **4b**: $[\alpha]_D^{20}$ = +25.5° (*c* 1.2, MeOH); mp 197−199 °C.

Data for (3*S*,3′*R*)-3-methylspiro[(dihydropyrazine-2,5-dione)-6,3′-(2′,3′-dihydrothieno[2,3-*b*]naphtho-4′,9′-dione)] (5a): FC in 20% MeOH in $CHCl_3$; yellow solid (32%); mp 205−206 °C; HPLC t_R 17.22 min; $[\alpha]_D^{20}$ = −7.5 (*c* 1.1, MeOH). ^{1}H NMR (500 MHz, CD_3OD): δ, 1.23 (m, 3H, C*H*$_3$), 3.40 (d, 1H, J = 12.8 Hz, H-2′^{b}), 3.52−3.56 (m, 1H, H-3), 3.58 (d, 1H, H-2′^{a}), 7.67−7.73 (m, 2H, H-6′ and H-7′), 8.00 (d, 1H, J = 7.4 Hz, H-8′); 8.03 (d, 1H, J = 7.5 Hz, H-5′). FAB-MS *m*/*z* calc for $C_{16}H_{12}N_2O_4S$ 328.34, found 328.39.

3(*S*),3′*S*)-3-Methylspiro[(dihydropirazin-2,5-dione)-6,3′-(2′,3′-dihydrothieno[2,3-*b*]naphtho-4′,9′-dione)] (5b). FC in 20% MeOH

in $CHCl_3$. Yellow solid (28%), mp 210−211 °C. HPLC t_R 16.31 min. $[\alpha]_D^{20} = +36.1$ (*c* 1.0, MeOH); ^{1}H NMR (500 MHz, CD_3OD) δ 1.22 (m, 3H, C*H*$_3$), 3.53 (d, 1H, *J* = 12.9 Hz, H-2′^{b}), 3.56 (d, 1H, H-2′^{a}), 3.59−3.62 (m, 1H, H-3), 7.83−7.89 (m, 2H, H-6′ and H-7′), 7.90 (d, 1H, *J* = 7.4 Hz, H-8′), 8.01 (d, 1H, *J* = 7.5 Hz, H-5′); FAB-MS *m*/*z* calcd for $C_{16}H_{12}N_2O_4S$ 328.34, found 328.51.

Data for (3*S*,3′*R*)-3-*sec*-butylspiro[(dihydropyrazine-2,5-dione)-6,3′-(2′,3′-dihydrothieno[2,3-*b*]naphtho-4′,9′-dione)] (6a): FC in AcOEt; yellow solid (27%); mp 223−224 °C; HPLC t_R 22.51 min; $[\alpha]_D^{20} = -9.0$ (*c* 1.0, MeOH); ^{1}H NMR (500 MHz, $CDCl_3$) δ 1.26 (s, 6H, H-δ), 1.69−1.75 (m, 1H, H-γ), 1.79−1.82 (m, 1H, H-β), 1.89−1.93 (m, 1H, H-β), 3.34 (d, 1H, *J* = 12.9 Hz, H-2′^{b}), 4.37 (d, 1H, H-2′^{a}), 4.46−4.49 (m, 1H, H-3), 6.32 (s, 1H, NH), 6.70 (s, 1H, NH), 7.67−7.73 (m, 2H, H-6′ and H-7′), 8.05 (d, 1H, *J* = 7.5 Hz, H-8′), 8.09 (d, 1H, *J* = 7.5 Hz, H-5′); FAB-MS *m*/*z* calcd for $C_{19}H_{18}N_2O_4S$ 370.42, found 370.63.

Data for (3*S*,3′*S*)-3-*sec*-butylspiro[(dihydropyrazine-2,5-dione)-6,3′-(2′,3′-dihydrothieno[2,3-*b*]naphtho-4′,9′-dione)] (6b): FC in AcOEt; yellow solid (23%); mp 226−228 °C; HPLC t_R 21.20 min; $[\alpha]_D^{20} = +31.7$ (*c* 1.0, MeOH); ^{1}H NMR (500 MHz, $CDCl_3$) δ 1.26 (s, 6H, H-δ), 1.87−1.94 (m, 1H, H-γ), 1.95−2.05 (m, 1H, H-β), 2.17−2.21 (m, 1H, H-β), 3.38 (d, 1H, *J* = 12.9 Hz, H-2′^{b}), 4.14−4.16 (m, 1H, H-3), 4.25 (d, 1H, H-2′^{a}), 6.26 (s, 1H, NH), 6.58 (s, 1H, NH), 7.68−7.75(m, 2H, H-6′ and H-7′), 8.03 (d, 1H, *J* = 7.4 Hz, H-8′), 8.08 (d, 1H, *J* = 7.5 Hz, H-5′); FAB-MS *m*/*z* calcd for $C_{19}H_{18}N_2O_4S$ 370.42, found 370.61.

Data for (3*S*,3′*R*)-3-spiro[(hexahydropyrrolo[1,2-*a*]pyrazine-1,4-dione)-6,3′-(2′,3′-dihydrothieno[2,3-*b*]naphtho-4′,9′-dione)] (7a): FC in AcOEt; yellow solid (30%); mp 199−203 °C; $[\alpha]_D^{20} = -98.3$ (*c* 1.2, MeOH); HPLC t_R 20.68 min; ^{1}H NMR (500 MHz, DMSO-d_6) δ 1.81−1.83 (m, 1H, H-γ), 1.87−1.90 (m, 2H, H-γ and H-β), 2.13−2.15 (m, 1H, H-β), 3.19−3.21 (m, 1H, H-δ), 3.43 (d, 1H, *J* = 12.6 Hz, H-2′^{b}), 3.59−3.61 (m, 1H, H-δ), 4.12 (d, 1H, H-2′^{a}), 4.41−4.43 (m, 1H, H-3), 7.83−7.86 (m, 2H, H-6′ and H-7′), 8.00 (d, 1H, *J* = 7.5 Hz, H-8′), 8.03 (d, 1H, *J* = 7.4 Hz, H-5′), 8.91(s, 1H, NH); ^{1}H NMR (500 MHz, $CDCl_3$) δ 1.99−2.15(m, 3H, H-β and H-γ), 2.47−2.51 (m, 1H, H-β), 3.27 (d, 1H, *J* = 12.6 Hz, H-2′^{b}), 3.69−3.73 (m, 2H, H-δ), 4.61 (d, 1H, H-2′^{a}), 4.64−4.66 (m, 1H, H-3), 6.69 (s, 1H, NH), 7.69−7.75 (m, 2H, H-6′ and H-7′), 7.99 (d, 1H, *J* = 7.4 Hz, H-8′), 8.06 (d, 1H, *J* = 7.4 Hz, H-5′); FAB-MS *m*/*z* calcd for $C_{18}H_{14}N_2O_4S$ 354.38, found 354.50.

Data for (3*S*,3′*S*)-spiro[(hexahydropyrrolo[1,2-*a*]pyrazine-1,4-dione)-6,3′-(2′,3′-dihydrothieno[2,3-*b*]naphtho-4′,9′-dione)] (7b): FC in AcOEt; yellow solid (23%); mp 210−212 °C; HPLC t_R 18.57 min; $[\alpha]_D^{20} = -74.6$ (*c* 1.0, MeOH); ^{1}H NMR (500 MHz, DMSO-d_6) δ 1.97−2.02 (m, 2H, H-γ), 2.05−2.08 (m, 1H, H-β), 2.13−2.15 (m, 1H, H-β), 3.40−3.43 (m, 1H, H-δ), 3.44−3.47 (m, 1H, H-δ), 3.90 (d, 1H, *J* = 12.6 Hz, H-2′^{b}), 3.95 (d, 1H, H-2′^{a}), 4.47−4.50 (m, 1H, H-3), 8.06−8.15 (m, 2H, H-6′ and H-7′), 8.18 (d, 1H, *J* = 7.4 Hz, H-8′), 8.21 (d, 1H, *J* = 7.4 Hz, H-5′), 8.93 (s, 1H, NH); ^{1}H NMR (500 MHz, $CDCl_3$) δ 1.80−1.84 (m, 1H, H-γ), 1.92−2.06 (m, 2H, H-β, H-γ), 2.33−2.36 (m, 1H, H-β), 3.32 (d, 1H, *J* = 12.6 MHz, H-2′^{b}), 3.49−3.51 (m, 1H, H-δ), 3.84−3.86 (m, 1H, H-δ), 4.11 (d, 1H, H-2′^{a}), 4.14−4.16 (m, 1H, H-3′), 6.77 (s, 1H, NH), 7.70−7.73 (m, 2H, H-6′ and H-7′), 8.01 (d, 1H, *J* = 7.4 Hz, H-8′), 8.08 (d, 1H, *J* = 7.4 Hz, H-5′); FAB-MS *m*/*z* calcd for $C_{18}H_{14}N_2O_4S$ 354.38, found 354.51.

Data for (3*S*,3′*R*)-3-benzylspiro[(dihydropyrazine-2,5-dione)-6,3′-(2′,3′-dihydrothieno[2,3-*b*]naphtho-4′,9′ -dione)] (8a): FC in 5% MeOH in $CHCl_3$; yellow solid (20%); mp 249−251 °C; HPLC t_R 23.15 min; $[\alpha]_D^{20} = -51.0$ (*c* 1.0, MeOH); ^{1}H NMR (500 MHz, DMSO-d_6) δ 3.10−3.14 (m, 2H, H-β), 3.61 (d, 1H, *J* = 12.6 Hz, H-2′^{b}), 3.83 (d, 1H, H-2′^{a}), 4.38−4.40 (m, 1H, H-3), 7.24−7.31 (m, 5H, aryl), 7.83−7.85 (m, 2H, H-6′ and H-7′), 7.92 (d, 1H, *J* = 7.5 Hz, H-8′), 7.98 (d, 1H, *J* = 7.4 Hz, H-5′), 8.71 (s, 1H, NH), 8.83 (s, 1H, NH); ^{1}H NMR (500 MHz, Cl_3CD) δ 2.60 (d, 1H, *J* = 12.9 Hz, H-2′^{b}), 3.11−3.15 (m, 1H, H-β), 3.33−3.36 (m, 1H, H-β), 3.97 (d, 1H, H-2′^{a}), 4.66−4.71 (m, 1H, H-3), 6.33 (s, 1H, NH), 6.57 (s, 1H, NH), 7.29−7.38 (m, 5H, aryl), 7.68−7.74 (m, 2H, H-6′ and H-7′), 7.98 (d, 1H, *J* = 7.3 Hz, H-8′), 8.06 (d, 1H, *J* = 7.4 Hz, H-5′); FAB-MS *m*/*z* calcd for $C_{22}H_{16}N_2O_4S$ 404.44, found 404.63.

Data for (3*S*,3′*S*)-3-benzylspiro[(dihydropyrazine-2,5-dione)-6,3′-(2′,3′-dihydrothieno[2,3-*b*]naphtho-4′,9′-dione)] (8b): FC in 5% MeOH in $CHCl_3$; yellow solid (26%); mp 263−265 °C; HPLC t_R 23.74 min; $[\alpha]_D^{20} = -8.3$ (*c* 1.1, MeOH); ^{1}H NMR (500 MHz, DMSO-d_6) δ 3.08−3.12 (m, 2H, H-β), 3.62 (d, 1H, *J* = 12.6 Hz, H-2′^{b}), 3.87 (d, 1H, H-2′^{a}), 4.40−4.42 (m, 1H, H-3), 7.22−7.30 (m, 5H, aryl), 7.83−7.85 (m, 2H, H-6′ and H-7′), 8.01 (d, 1H, *J* = 7.5 Hz, H-8′), 8.03 (d, 1H, *J* = 7.4 Hz, H-5′), 8.38 (s, 1H, NH), 8.80 (s, 1H, NH); ^{1}H NMR (500 MHz, $CDCl_3$) δ 3.38 (d, 1H, *J* = 12.9 Hz, H-2′^{b}), 3.45−3.47 (m, 1H, H-β), 3.51−3.53 (m, 1H, H-β), 4.21−4.23 (m, 1H, H-3), 4.26 (d, 1H, H-2′^{a}), 6.18 (s, 1H, NH), 6.30 (s, 1H, NH), 7.29−7.38 (m, 5H, aryl), 7.68−7.78 (m, 2H, H-6′ and H-7′), 8.05 (d, 1H, *J* = 7.4 Hz, H-8′), 8.11 (d, 1H, *J* = 7.4 Hz, H-5′); FAB-MS *m*/*z* calcd for $C_{22}H_{16}N_2O_4S$ 404.44, found 404.51.

Data for (3*S*,3′*R*)-3-[4-(*tert*-butyloxy)benzyl]spiro[(dihydropyrazine-2,5-dione)-6,3′-(2′,3′-dihydrothieno[2,3-*b*]naphtho-4′,9′-dione)] (9′a): FC in AcOEt; yield 24%; ^{1}H NMR (500 MHz, $CDCl_3$) δ 1.32 (s, 9H, C*H*$_3$), 2.68 (d, 1H, *J* = 12.9 Hz, H-2′^{b}), 3.11−3.15 (m, 1H, H-β), 3.28−3.32 (m, 1H, H-β), 4.05 (d, 1H, H-2′^{a}), 4.66−4.71 (m, 1H, H-3), 6.07 (s, 1H, NH), 6.24 (s, 1H, NH), 7.00 (d, 2H, *J* = 6.8 Hz, aryl), 7.19 (d, 2H, *J* = 6.9 Hz, aryl), 7.70−7.74 (m, 2H, H-6′ and H-7′), 8.00 (d, 1H, *J* = 7.4 Hz, H-8′), 8.06 (d, 1H, *J* = 7.5 Hz, H-5′). After removal of the *tert*-butyl group the corresponding (3*S*,3′*R*)-3-(4-hydroxybenzyl)spiro-[(dihydropyrazine-2,5-dione)-6,3′-(2′,3′-dihydrothieno[2,3-*b*]naphtho-4′,9′-dione)] (**9a**) was quantitatively obtained as a yellow solid: mp 282−283 °C; HPLC t_R 28.2 min; $[\alpha]_D^{20} = -32.0$ (*c* 2.0, MeOH); ^{1}H NMR (500 MHz, DMSO-d_6) δ 2.72−2.74 (m, 1H, H-β), 3.03−3.05 (m, 1H, H-β), 3.73 (d, 1H, *J* = 12.6 Hz, H-2′^{b}), 3.82 (d, 1H, H-2′^{a}), 4.38−4.40 (m, 1H, H-3), 6.95 (d, 2H, *J* = 7.4 Hz, aryl), 7.12 (d, 2H, *J* = 7.4 Hz, aryl), 7.804−7.87 (m, 2H, H-6′ and H-7′), 7.97 (d, 1H, *J* = 7.5 Hz, H-8′), 8.01 (d, 1H, *J* = 7.4 Hz, H-5′), 8.72 (s, 1H, NH), 8.79 (s, 1H, NH); ^{1}H NMR (500 MHz, $CDCl_3$) δ 2.68 (d, 1H, *J* = 12.9 Hz, H-2′^{b}), 3.11−3.15 (m, 1H, H-β), 3.28−3.32 (m, 1H, H-β), 4.03 (d, 1H, H-2′^{a}), 4.66−4.69 (m, 1H, H-3), 6.07 (s, 1H, NH), 6.24 (s, 1H, NH), 7.00 (d, 2H, *J* = 6.9 Hz, aryl), 7.19 (d, 2H, *J* = 6.9 Hz, aryl), 7.70−7.74 (m, 2H, H-6′ and H-7′), 8.00 (d, 1H, *J* = 7.4 Hz, H-8′), 8.08 (d, 1H, *J* = 7.4 Hz, H-5′); FAB-MS *m*/*z* calcd for $C_{22}H_{16}N_2O_5S$ 420.44, found 420.41.

Data for (3*S*,3′*S*)-3-[4-(*tert*-butyloxy)benzyl]spiro[(dihydropyrazine-2,5-dione)-6,3′-(2′,3′-dihydrothieno[2,3-*b*]naphtho-4′,9′-dione)] (9′b): FC in AcOEt; yield 32%; ^{1}H NMR (500 MHz, $CDCl_3$) δ 1.32 (s, 9H, C*H*$_3$), 3.40 (d, 1H, *J* = 12.8 Hz, H-2′^{b}), 3.45−3.47 (m, 2H, H-β), 4.21−4.23 (m, 1H, H-3), 4.29 (d, 1H, H-2′^{a}), 5.89 (s, 1H, NH), 6.51 (s, 1H, NH), 7.03 (d, 2H, *J* = 7.4 Hz, aryl), 7.33 (d, 2H, *J* = 7.4 Hz, aryl), 7.70−7.78 (m, 2H, H-6′ and H-7′), 8.10−8.13 (m, 2H, H-8′ and H-5′). After removal of the *tert*-butyl group the corresponding (3*S*,3′*S*)-3-(4-hydroxybenzyl)-spiro[(dihydropyrazine-2,5-dione)-6,3′-(2′,3′-dihydrothieno[2,3-*b*]-naphtho-4′,9′-dione)] (**9b**) was obtained as a yellow solid (91%): mp 293−294 °C; HPLC t_R 29.6 min; $[\alpha]_D^{20} = +11.1$ (*c* 1.5, MeOH); ^{1}H NMR (500 MHz, DMSO-d_6) δ 3.04−3.06 (m, 1H, H-β), 3.08−3.10 (m, 1H, H-β), 3.69 (d, 1H, *J* = 12.6 Hz, H-2′^{b}), 3.82 (d, 1H, H-2′^{a}), 4.38−4.40 (m, 1H, H-3), 6.90 (d, 2H, *J* = 7.4 Hz, aryl), 7.23 (d, 2H, *J* = 7.4 Hz, aryl), 7.84−7.89 (m, 2H, H-6′ and H-7′), 7.98 (d, 1H, *J* = 7.5 Hz, H-8′), 8.03 (d, 1H, *J* = 7.4 Hz, H-5′), 8.41 (s, 1H, NH), 8.79 (s, 1H, NH); ^{1}H NMR (500 MHz, $CDCl_3$) δ 3.36 (d, 1H, *J* = 12.8 Hz, H-2′^{b}), 3.40−3.44 (m, 2H, H-β), 4.19−4.21 (m, 1H, H-3), 4.27 (d, 1H, H-2′^{a}), 6.00 (s, 1H, NH), 6.58 (s, 1H, NH), 7.03 (d, 2H, *J* = 7.4 Hz, aryl), 7.33 (d, 2H, *J* = 7.4 Hz, aryl), 7.70−7.78 (m, 2H, H-6′ and H-7′), 8.00 (d, 1H, *J* = 7.4 Hz, H-8′), 8.03 (d, 1H, *J* = 7.4 Hz, H-5′); FAB-MS *m*/*z* calcd for $C_{22}H_{16}N_2O_5S$ 420.44, found 420.41.

Data for (3*S*,3′*R*)-3-[(*tert*-butyloxy)methyl]spiro[dihydropyrazine-2,5-dione-6,3′-(2′,3′-dihydrothieno[2,3-*b*]naphtho-4′,9′-dione)] (10′a): FC in AcOEt; yield 26%; ^{1}H NMR (500 MHz, $CDCl_3$) δ 1.40 (s, 9H, C*H*$_3$), 3.41 (d, 1H, *J* = 12.6 Hz, H-2′^{b}), 3.69−3.72

(m, 1H, H-β), 3.82−3.84 (m, 1H, H-β), 4.35 (d, 1H, H-2′^{a}), 4.58−4.60 (m, 1H, H-3), 6.57 (s, 1H, NH), 6.64 (s, 1H, NH), 7.69−7.75 (m, 2H, H-6′ and H-7′), 8.00 (d, 1H, J = 7.3 Hz, H-8′), 8.07 (d, 1H, J = 7.4 Hz, H-5′). After removal of the *tert*-butyl group the corresponding (3*S*,3′*R*)-3-(hydroxymethyl)spiro[dihydropyrazine-2,5-dione-6,3′-(2′,3′-dihydrothieno[2,3-*b*]naphtho-4′,9′-dione)] (**10a**) was obtained as a yellow solid (91%); mp 239−241 °C; HPLC t_R 22.97 min; $[\alpha]_D^{20}$ = −9.8 (*c* 0.8, MeOH); ^{1}H NMR (500 MHz, CD_3OD) δ 3.59 (d, 1H, J = 12.6 Hz, H-2′^{b}), 3.60−3.63 (m, 1H, H-β), 3.84−3.86 (m, 1H, H-β), 4.01 (d, 1H, H-2′^{a}), 4.20−4.23 (m, 1H, H-3), 7.77−7.82 (m, 2H, H-6′ and H-7′), 8.04 (d, 1H, J = 7.4 Hz, H-8′), 8.09 (d, 1H, J = 7.4 Hz, H-5′); FAB-MS *m*/*z* calcd for $C_{16}H_{12}N_2O_5S$ 344.34, found 344.51.

Data for (3*S*,3′*S*)-3-[(*tert*-butyloxy)methyl]spiro[dihydropyrazine-2,5-dione-6,3′-(2′,3′-dihydrothieno[2,3-*b*]naphtho-4′,9′-dione)] (10′b): FC in AcOEt; yield 26%; ^{1}H NMR (500 MHz, $CDCl_3$) δ 1.40 (s, 9H, CH_3), 3.41 (d, 1H, J = 12.6 Hz, H-2′^{b}), 3.91−3.94 (m, 1H, H-β), 4.03−4.07 (m, 1H, H-β), 4.26−4.30 (m, 2H, H-2′^{a} and H-3), 6.35 (s, 1H, NH), 6.38 (s, 1H, NH), 7.67−7.75 (m, 2H, H-6′ and H-7′), 8.03 (d, 1H, J = 7.4 Hz, H-8′), 8.08 (d, 1H, J = 7.4 Hz, H-5′). After removal of the *tert*-butyl group the corresponding (3*S*,3′*S*)-3-(hydroxymethyl)spiro[dihydropyrazine-2,5-dione-6,3′-(2′,3′-dihydrothieno[2,3-*b*]naphtho-4′,9′-dione)] (**10b**) was obtained as a yellow solid (90%): mp 248−249 °C; HPLC t_R 23.74 min; $[\alpha]_D^{20}$ = +33.6 (*c* 1.0, MeOH); ^{1}H NMR (500 MHz, CD_3-OD) δ 3.60 (d, 1H, J = 12.6 Hz, H-2′^{b}), 3.74−3.76 (m, 1H, H-β), 4.00−4.03 (m, 1H, H-β), 4.11 (d, 1H, H-2′^{a}), 4.16−4.19 (m, 1H, H-3), 7.77−7.83 (m, 2H, H-6′ and H-7′), 8.04 (d, 1H, J = 7.4 Hz, H-8′), 8.08 (d, 1H, J = 7.4 Hz, H-5′); FAB-MS *m*/*z* calcd for $C_{16}H_{12}N_2O_5S$ 344.34, found 344.51.

Data for (3*R*,3′*R*)-3-[(tritylthio)methyl]spiro[dihydropyrazine-2,5-dione-6,3′-(2′,3′-dihydrothieno[2,3-*b*] naphtho-4′,9′-dione)] (11′a): FC in AcOEt; yield 26%; ^{1}H NMR (500 MHz, $CDCl_3$) δ 2.79−2.89 (m, 2H, H-β), 3.26 (d, 1H, J = 12.6 Hz, H-2′^{b}), 3.98−4.00 (m, 1H, H-3), 4.28 (d, 1H, H-2′^{a}), 5.99 (s, 1H, NH), 6.54 (s, 1H, NH), 7.26−7.48 and 7.50−7.54 (m, 15H, aryl), 7.67−7.75 (m, 2H, H-6′ and H-7′), 8.00 (d, 1H, J = 7.4 Hz, H-8′), 8.05 (d, 1H, J = 7.4 Hz, H-5′). After removal of the trityl group the corresponding (3*R*,3′*R*)-3-(mercaptomethyl)spiro[(dihydropyrazine-2,5-dione)-6,3′-(2′,3′-dihydrothieno[2,3-*b*]naphtho-4′,9′-dione)] (**11a**) was obtained as a yellow solid (80%): mp 181−183 °C; HPLC t_R 21.69 min; $[\alpha]_D^{20}$ = −16.2 (*c* 1.5, MeOH); ^{1}H NMR (500 MHz, CD_3OD) δ 3.11−3.15 (m, 2H, H-β), 3.64 (d, 1H, J = 12.6 Hz, H-2′^{b}), 4.23 (d, 1H, H-2′^{a}), 4.34−4.36 (m, 1H, H-3), 7.77−7.83 (m, 2H, H-6′ and H-7′), 8.05 (d, 1H, J = 7.4 Hz, H-8′), 8.09 (d, 1H, J = 7.4 Hz, H-5′); FAB-MS *m*/*z* calcd for $C_{16}H_{12}N_2O_4S_2$ 360.40, found 360.25.

Data for (3*R*,3′*S*)-3-[(tritylthio)methyl]spiro[dihydropyrazine-2,5-dione-6,3′-(2′,3′-dihydrothieno[2,3-*b*]naphtho-4′,9′-dione)] (11′b): FC in AcOEt; yield 20%; ^{1}H NMR (500 MHz, $CDCl_3$) δ 3.07−3.18 (m, 2H, H-β), 3.25 (d, 1H, J = 12.7 Hz, H-2′^{b}), 3.49−3.52 (m, 1H, H-3), 4.18 (d, 1H, H-2′^{a}), 6.22 (s, 1H, NH), 6.36 (s, 1H, NH), 7.20−7.538 (m, 15H, aryl), 7.66−7.73 (m, 2H, H-6′ and H-7′), 8.00 (d, 1H, J = 7.4 Hz, H-8′), 8.05 (d, 1H, J = 7.4 Hz, H-5′). After removal of the trityl group the corresponding (3*R*,3′*S*)-3-(mercaptomethyl)spiro[(dihydropyrazine-2,5-dione)-6,3′-(2′,3′-dihydrothieno[2,3-*b*]naphtho-4′,9′-dione)] (**11b**) was obtained as a yellow solid (82%): mp 198−201 °C; HPLC t_R 20.56 min; $[\alpha]_D^{20}$ = +27.9 (*c* 1.1, MeOH); ^{1}H NMR (500 MHz, CD_3OD) δ 3.14−3.16 (m, 1H, H-β), 3.19−3.21 (m, 1H, H-β), 3.58 (d, 1H, J = 12.6 Hz, H-2′^{b}), 4.09 (d, 1H, H-2′^{a}), 4.15−4.18 (m, 1H, H-3), 7.77−7.83 (m, 2H, H-6′ and H-7′), 8.05 (d, 1H, J = 7.4 Hz, H-8′), 8.09 (d, 1H, J = 7.4 Hz, H-5′); FAB-MS *m*/*z* calcd for $C_{16}H_{12}N_2O_4S_2$ 360.40, found 360.26.

Data for (3*S*,3′*R*)-3-[(methylthio)ethyl]spiro[dihydropyrazine-2,5-dione-6,3′-(2′,3′-dihydrothieno[2,3-*b*]naphtho-4′,9′-dione)] (12a): FC in AcOEt; yellow solid (26%); mp 242−244 °C; HPLC t_R 21.86 min; $[\alpha]_D^{20}$ = −3.0 (*c* 1.0, MeOH); ^{1}H NMR (500 MHz, $CDCl_3$) δ 2.10 (s, 3H, CH_3), 2.26−2.29 (m, 2H, H-β), 2.64−2.74 (m, 2H, H-γ), 3.28 (d, 1H, J = 12.9 Hz, H-2′^{b}), 4.40 (d, 1H, H-2′^{a}), 4.54−4.60 (m, 1H, H-3), 6.40 (s, 1H, NH), 6.63 (s, 1H, NH), 7.69−7.73 (m, 2H, H-6′ and H-7′), 8.00 (d, 1H, J = 7.4 Hz, H-8′), 8.07 (d, 1H, J = 7.4 Hz, H-5′); FAB-MS *m*/*z* calcd for $C_{18}H_{16}N_2O_4S_2$ 388.46, found 388.31.

Data for (3*S*,3′*S*)-3-[(methylthio)ethyl]spiro[dihydropyrazine-2,5-dione-6,3′-(2′,3′-dihydrothieno[2,3-*b*]naphtho-4′,9′-dione)] (12b): FC in AcOEt; yellow solid (26%); mp 251−253 °C; HPLC t_R 20.80 min; $[\alpha]_D^{20}$ = +39.1 (*c* 1.1, MeOH); ^{1}H NMR (500 MHz, $CDCl_3$) δ 2.12 (s, 3H, CH_3), 2.36−2.40 (m, 2H, H-β), 2.71−2.76 (m, 2H, H-γ), 3.31 (d, 1H, J = 12.8 Hz, H-2′^{b}), 4.12 (d, 1H, H-2′^{a}), 4.28−4.32 (m, 1H, H-3), 6.45 (s, 1H, NH), 6.83 (s, 1H, NH), 7.70−7.76 (m, 2H, H-6′ and H-7′), 8.01 (d, 1H, J = 7.4 Hz, H-8′), 8.11 (d, 1H, J = 7.4 Hz, H-5′); FAB-MS *m*/*z* calcd for $C_{18}H_{16}N_2O_4S_2$ 388.46, found 388.29.

Data for (3*S*,3′*R*)-3-[(*N*-(*tert*-butyloxycarbonyl)amino)butyl]-spiro[(dihydropyrazine-2,5-dione)-6,3′-(2′,3′-dihydrothieno[2,3-*b*]naphtho-4′,9′-dione)] (13′a): FC in AcOEt; yield 22%; ^{1}H NMR (500 MHz, $CDCl_3$) δ 1.41 (s, 9H, CH_3), 1.52−1.55 (m, 4H, H-γ and H-δ), 1.94−1.96 (m, 2H, H-β), 3.11−3.14 (m, 2H, H-ϵ), 3.36 (d, 1H, J = 12.9 Hz, H-2′^{b}); 4.36 (d, 1H, H-2′^{a}), 4.50−4.52 (m, 1H, H-3), 4.64 (s, 1H, N*H*Boc), 6.61 (s, 1H, N*H*), 6.85 (s, 1H, N*H*), 7.66−7.72 (m, 2H, H-6′ and H-7′), 7.97 (d, 1H, J = 7.4 Hz, H-8′), 8.05 (d, 1H, J = 7.4 Hz, H-5′). After removal of the *N*-Boc protecting group the corresponding (3*S*,3′*R*)-3-(aminobutyl)spiro-[(dihydropyrazine-2,5-dione)-6,3′-(2′,3′-dihydrothieno[2,3-*b*]naphtho-4′,9′-dione)] trifluoroacetate (**13a**) was quantitatively obtained as a yellow solid: mp 244−246 °C; HPLC t_R 14.52 min; $[\alpha]_D^{20}$ = −2.2 (*c* 1.0, water); ^{1}H NMR (500 MHz, CD_3OD) δ 1.02−1.07 (m, 2H, H-γ), 1.44−1.56 (m, 4H, H-δ and H-β), 2.79−2.82 (m, 2H, H-ϵ), 3.47 (d, 1H, J = 12.6 Hz, H-2′^{b}), 4.16 (d, 1H, H-2′^{a}), 4.50−4.52 (m, 1H, H-3), 7.76−7.79 (m, 2H, H-6′ and H-7′), 8.01 (d, 1H, J = 7.4 Hz, H-8′), 8.05 (d, 1H, J = 7.4 Hz, H-5′); FAB-MS *m*/*z* calcd for $C_{19}H_{19}N_3O_4S$·TFA 499.10, found 499.14.

Data for (3*S*,3′*S*)-3-[(*N*-(*tert*-butyloxycarbonyl)amino)butyl]-spiro[(dihydropyrazine-2,5-dione)-6,3′-(2′,3′-dihydrothieno[2,3-*b*]naphtho-4′,9′-dione)] (13′b): FC in AcOEt; yield 20%; ^{1}H NMR (500 MHz, $CDCl_3$) δ 1.40 (s, 9H, CH_3), 1.99−2.04 (m, 2H, H-γ), 2.16−2.23 (m, 2H, H-δ), 3.11−3.15 (m, 2H, H-β), 3.19−3.21 (m, 2H, H-ϵ), 3.39 (d, 1H, J = 12.9 Hz, H-2′^{b}), 4.14−4.16 (m, 1H, H-3), 4.20 (d, 1H, H-2′^{a}), 4. 84 (s, 1H, N*H*Boc), 6.72 (s, 1H, N*H*), 6.88 (s, 1H, N*H*), 7.66−7.73 (m, 2H, H-6′ and H-7′), 8.01 (d, 1H, J = 7.3 Hz, H-8′), 8.06 (d, 1H, J = 7.4 Hz, H-5′). After removal of the *N*-Boc group the corresponding (3*S*,3′*S*)-3-(aminobutyl)spiro-[(dihydropyrazine-2,5-dione)-6,3′-(2′,3′-dihydrothieno[2,3-*b*]naphtho-4′,9′-dione)] trifluoroacetate (**13b**) was quantitatively obtained as a yellow solid: mp 251−253 °C; HPLC t_R 11.27 min; $[\alpha]_D^{20}$ = +42.7 (*c* 1.0, water); ^{1}H NMR (500 MHz, CD_3OD) δ 1.02−1.07 (m, 2H, H-γ), 1.44−1.56 (m, 4H, H-δ and H-β), 2.79−2.82 (m, 2H, H-ϵ), 3.47 (d, 1H, J = 12.6 Hz, H-2′^{b}), 4.16 (d, 1H, H-2′^{a}), 4.50−4.52 (m, 1H, H-3), 7.76−7.79 (m, 2H, H-6′ and H-7′), 8.01 (d, 1H, J = 7.4 Hz, H-8′), 8.05 (d, 1H, J = 7.4 Hz, H-5′); FAB-MS *m*/*z* calcd for $C_{19}H_{19}N_3O_4S$·TFA 499.10, found 499.27

Data for (3*S*,3′*R*)-3-[(1-trityl-1*H*-imidazol-4-yl)methyl]spiro-[dihydropyrazine-2,5-dione-6,3′-(2′,3′-dihydrothieno[2,3-*b*]naphtho-4′,9′-dione)] (14′a): FC in AcOEt; yield 20%; ^{1}H NMR (500 MHz, $CDCl_3$) δ 2.86−2.93 (m, 1H, H-β), 3.27 (d, 1H, J = 12.8 Hz, H-2′^{b}), 3.32−3.35 (m, 1H, H-β), 4.41 (d, 1H, H-2′^{a}), 4.69−4.71 (m, 1H, H-3), 6.63 (s, 1H, NH), 6.70 (s, 1H, NH), 7.02−7.35 (m, 15H, aryl), 7.40 (s, 1H, imidazole), 7.66−7.73 (m, 2H, H-6′, H-7′), 7.98 (d, 1H, J = 7.3 Hz, H-8′), 8.06 (d, 1H, J = 7.3 Hz, H-5′), 8.23 (s, 1H, imidazol). After removal of the trityl group the corresponding (3*S*,3′*R*)-3-(1*H*-imidazol-4-ylmethyl)spiro[dihydropyrazine-2,5-dione-6,3′-(2′,3′-dihydrothieno[2,3-*b*]naphtho-4′,9′-dione)] (**14a**) was quantitatively obtained as a yellow solid: mp 259−261 °C; HPLC t_R 17.77 min; $[\alpha]_D^{20}$ = −18.8 (*c* 1.0, MeOH); ^{1}H NMR (500 MHz, DMSO-d_6) δ 3.08−3.14 (m, 2H, H-β), 3.57 (d, 1H, J = 12.6 Hz, H-2′^{b}), 3.921 (d, 1H, H-2′^{a}), 4.40−4.41 (m, 1H, H-3), 7.20 (s, 1H, imidazole), 7.83−7.86 (m, 2H, H-6′ and H-7′), 8.01 (d, 1H, J = 7.5 Hz, H-8′), 8.04 (d, 1H, J = 7.4 Hz, H-5′), 8.61 (s, 1H, imidazole), 8.92 (s, 1H, NH), 9.00 (s, 1H, NH); ^{1}H NMR (500 MHz, CD_3OD) δ 2.96 (d, 1H, J = 12.8 Hz, H-2′^{b}), 3.14−3.19 (m, 1H, H-β), 3.27−3.30 (m, 1H, H-β), 3.89 (d, 1H, H-2′^{a}), 4.56−4.60 (m, 1H, H-3), 7.20 (s, 1H, imidazole), 7.68−

7.72 (m, 2H, H-6′, H-7′), 7.92 (d, 1H, J = 7.3 Hz, H-8′), 7.97 (d, 1H, J = 7.3 Hz, H-5′), 8.37 (s, 1H, imidazole); FAB-MS *m*/*z* calcd for $C_{19}H_{14}N_4O_4S$ 394.41, found 394.53.

Data for (3*S*,3′*S*)-3-[(1-trityl-1*H*-imidazol-4-yl)methyl]spiro-[dihydropyrazine-2,5-dione-6,3′-(2′,3′-dihydrothieno[2,3-*b*]naphtho-4′,9′-dione)] (14′b): FC in AcOEt; yield 20%; ^{1}H NMR (500 MHz, $CDCl_3$) δ 3.10−3.13 (m, 1H, H-β), 3.19−3.23 (m, 1H, CH_2), 3.38 (d, 1H, J = 12.8 Hz, H-2′^{b}), 4.24 (d, 1H, H-2′^{a}), 4.38−4.41 (m, 1H, H-3), 6.61 (s, 1H, NH), 6.65 (s, 1H, NH), 7.02−7.35 (m, 15H, aryl), 7.39 (s, 1H, imidazole), 7.61−7.63 (t, 1H, J = 7.4 Hz, H-6′), 7.68−7.70 (t, 1H, J = 7.4 Hz, H-7′), 7.94−7.98 (m, 2H, H-8′ and H-5′), 8.27 (s, 1H, imidazole). After removal of the trityl group the corresponding (3*S*,3′*S*)-3-(1*H*-imidazol-4-ylmethyl)spiro-[dihydropyrazine-2,5-dione-6,3′-(2′,3 ′-dihydrothieno[2,3-*b*]naphtho-4′,9′-dione)] (**14b**) was quantitatively obtained as a yellow solid: mp 265−268 °C; HPLC t_R 16.54 min; $[\alpha]_D^{20}$ = +27.8 (*c* 1.0, MeOH); ^{1}H NMR (500 MHz, DMSO-d_6) δ 2.94−2.97 (m, 1H, H-β), 3.10−3.13 (m, 1H, H-β), 3.68 (d, 1H, J = 12.6 Hz, H-2′^{b}), 3.82 (d, 1H, H-2′^{a}), 4.18−4.20 (m, 1H, H-3), 6.96 (s, 1H, imidazole), 7.83−7.86 (m, 2H, H-6′ and H-7′), 8.03 (d, 1H, J = 7.5 Hz, H-8′), 8.06 (d, 1H, J = 7.4 Hz, H-5′), 8.42 (s, 1H, imidazole), 8.91(s, 1H, NH), 8.94(s, 1H, NH); ^{1}H NMR (500 MHz, CD_3OD) δ 3.10 (d, 1H, J = 12.8 Hz, H-2′^{b}), 3.19−3.23 (m, 1H, H-β), 3.29−3.32 (m, 1H, H-β), 3.38 (d, 1H, H-2′^{a}), 4.40−4.43 (m, 1H, H-3), 7.28 (s, 1H, imidazole), 7.69−7.74 (m, 2H, H-6′, H-7′), 7.91 (d, 1H, J = 7.4 Hz, H-8′), 7.97 (d, 1H, J = 7.4 Hz, H-5′), 8.35 (s, 1H, imidazole); FAB-MS *m*/*z* calcd for $C_{19}H_{14}N_4O_4S$ 394.41, found 394.53.

Data for (3*S*,3′*R*)-3-[(*tert*-butyloxycarbonyl)methyl]spiro-[(dihydropyrazine-2,5-dione)-6,3′-(2′,3′-dihydrothieno[2,3-*b*]-naphtho-4′,9′-dione)] (15′a): FC in AcOEt; yield 20%; ^{1}H NMR (500 MHz, $CDCl_3$) δ 1.48 (s, 9H, CH_3), 2.77−2.81 (m, 1H, H-β), 3.05−3.18 (m, 1H, H-β), 3.47 (d, 1H, J = 12.8 Hz, H-2′^{b}), 4.39 (d, 1H, H-2′^{a}), 4.75−4.77 (m, 1H, H-3), 6.60 (s, 1H, NH), 6.86 (s, 1H, NH), 7.66−7.73 (m, 2H, H-6′, H-7′), 8.00 (d, 1H, J = 7.4 Hz, H-8′), 8.10 (d, 1H, J = 7.4 Hz, H-5′). After removal of the *tert*-butyl group the corresponding (3*S*,3′*R*)-3-[(hydroxycarbonyl)-methyl]spiro[(dihydropyrazine-2,5-dione)-6,3′-(2′,3′-dihydrothieno-[2,3-*b*]naphtho-4′,9′-dione)] (**15a**) was obtained as a yellow solid (90%): mp 280−282 °C; HPLC t_R 13.2 min; $[\alpha]_D^{20}$ = +1.8 (*c* 1.0, MeOH); ^{1}H NMR (500 MHz, DMSO-d_6) δ 2.36−2.39 (m, 1H, H-β), 2.73−2.75 (m, 1H, H-β), 3.27 (d, 1H, J = 12.8 Hz, H-2′^{b}), 3.49 (d, 1H, H-2′^{a}), 4.32−4.35 (m, 1H, H-3), 7.68−7.74 (m, 2H, H-6′, H-7′), 7.86 (s, 1H, NH), 8.00 (d, 1H, J = 7.4 Hz, H-8′), 8.03 (s, 1H, NH), 8.10 (d, 1H, J = 7.4 Hz, H-5′); FAB-MS *m*/*z* calcd for $C_{17}H_{12}N_2O_6S$ 372.04, found 372.10.

Data for (3*S*,3′*S*)-3-[(*tert*-butyloxycarbonyl)methyl]spiro-[(dihydropyrazine-2,5-dione)-6,3′-(2′,3′-dihydrothieno[2,3-*b*]-naphtho-4′,9′-dione)] (15′b): FC in AcOEt; yield 20%; ^{1}H NMR (500 MHz, $CDCl_3$) δ 1.36 (s, 9H, CH_3), 3.08−3.20 (m, 1H, H-β), 3.45 (d, 1H, J = 12.8 Hz, H-2′^{b}), 3.46−3.49 (m, 1H, H-β), 4.30 (d, 1H, H-2′^{a}), 4.50−4.53 (m, 1H, H-3), 6.60 (s, 1H, NH), 6.90 (s, 1H, NH), 7.71−7.76 (m, 2H, H-6′, H-7′), 8.01 (d, 1H, J = 7.4 Hz, H-8′), 8.10 (d, 1H, J = 7.4 Hz, H-5′). After removal of the *tert*-butyl group the corresponding (3*S*,3′*S*)-3-[(hydroxycarbonyl)methyl]-spiro[(dihydropyrazine-2,5-dione)-6,3′-(2′,3′-dihydrothieno[2,3-*b*]-naphtho-4′,9′-dione)] (**15b**) was obtained as a yellow solid (93%): mp 291−292 °C; HPLC t_R 14.1 min; $[\alpha]_D^{20}$ +46.2 (*c* 1.00, MeOH); ^{1}H NMR (500 MHz, DMSO-d_6) δ 2.58−2.61 (m, 1H, H-β), 2.79−2.81 (m, 1H, H-β), 3.31 (d, 1H, J = 12.8 Hz, H-2′^{b}), 3.36 (d, 1H, H-2′^{a}), 4.54−4.57 (m, 1H, H-3), 7.66−7.73 (m, 2H, H-6′, H-7′), 7.78 (s, 1H, NH), 8.00 (d, 1H, J = 7.4 Hz, H-8′), 8.01 (s, 1H, NH), 8.10 (d, 1H, J = 7.4 Hz, H-5′); FAB-MS *m*/*z* calcd for $C_{17}H_{12}N_2O_6S$ 372.04, found 372.13.

Data for (3*S*,3′*R*)-3-[(*N*-Tritylaminocarbonyl)methyl]spiro-[(dihydropyrazine-2,5-dione)-6,3′-(2′,3′- dihydrothieno[2,3-*b*]-naphtho-4′,9′-dione)] (16a′): FC in AcOEt; yield 22%; ^{1}H NMR (500 MHz, $CDCl_3$) δ 2.85−2.90 (m, 1H, H-β), 3.08−3.13 (m, 1H, H-β), 3.21 (d, 1H, J = 12.8 Hz, H-2′^{b}), 4.20 (d, 1H, H-2′^{a}), 4.78−4.80 (m, 1H, H-3), 6.43 (s, 1H, NH), 6.89 (s, 1H, NH), 7.28−7.31 (m, 15H, aryl), 7.67−7.74 (m, 2H, H-6′ and H-7′), 7.99 (d, 1H, J = 7.4 Hz, H-8′,), 8.06 (d, 1H, J = 7.4 Hz, H-5′). After removal of the trityl group the corresponding (3*S*,3′*R*)-3-[(aminocarbonyl)-methyl]spiro[(dihydropyrazine-2,5-dione)-6,3′-(2′,3′-dihydrothieno-[2,3-*b*]naphtho-4′,9′-dione)] (**16a**) was quantitatively obtained as a yellow solid: mp 225−228 °C; HPLC t_R 18.21 min; $[\alpha]_D^{20}$ = +7.2 (*c* 1.5, MeOH); ^{1}H NMR (500 MHz, CD_3OD) δ 2.96−3.00 (m, 2H, H-β), 3.61 (d, 1H, J = 12.9 Hz, H-2′^{b}), 4.18 (d, 1H, H-2′^{a}), 4.41−4.46 (m, 1H, H-3), 7.76−7.83 (m, 2H, H-6′, H-7′), 8.02 (d, 1H, J = 7.4 Hz, H-8′), 8.06 (d, 1H, J = 7.4 Hz, H-5′); FAB-MS *m*/*z* calcd for $C_{17}H_{13}N_3O_5S$ 371.37, found 371.53.

Data for (3*S*,3′*S*)-3-[(*N*-Tritylaminocarbonyl)methyl]spiro-[(dihydropyrazine-2,5-dione)-6,3′-(2′,3′-dihydrothieno[2,3-*b*]-naphtho-4′,9′-dione)] (16b′): FC in AcOEt; yield 25%; ^{1}H NMR (500 MHz, $CDCl_3$) δ 2.90−2.94 (m, 1H, H-β), 2.99−3.023 (m, 1H, H-β), 3.30 (d, 1H, J = 12.9 Hz, H-2′^{b}), 4.19 (d, 1H, H-2′^{a}), 4.36−4.38 (m, 1H, H-3), 6.90 (s, 1H, NH), 7.14 (s, 1H, NH), 7.28−7.35 (m, 15H, aryl), 7.53−7.56 (m, 1H, H-6′), 7.61 (s, 1H, NH), 7.69−7.72 (m, 1H, H-7′), 7.84−7.86 (m, 2H, H-5′ and H-8′). After removal of the trityl group the corresponding (3*S*,3′*S*)-3-[(aminocarbonyl)methyl]spiro[(dihydropyrazine-2,5-dione)-6,3′-(2′,3′-dihydrothieno[2,3-*b*]naphtho-4′,9′-dione)] (**16b**) was quantitatively obtained as a yellow solid: mp 218−220 °C; HPLC t_R 18.53 min; $[\alpha]_D^{20}$ = +51.2 (*c* 1.0, MeOH); ^{1}H NMR (500 MHz, CD_3OD) δ 2.81−2.85 (m, 1H, H-β), 2.98−3.00 (m, 1H, H-β), 3.70 (d, 1H, J = 12.9 Hz, H-2′^{b}), 4.15 (d, 1H, H-2′^{a}), 4.50−4.52 (m, 1H, H-3), 7.78−7.85 (m, 2H, H-6′, H-7′), 8.04 (d, 1H, J = 7.4 Hz, H-8′), 8.08 (d, 1H, J = 7.4 Hz, H-5′); FAB-MS *m*/*z* calcd for $C_{17}H_{13}N_3O_5S$ 371.37, found 371.53.

Cell Lines. Human tumor cell lines were used in this study, NCI-H460 lung carcinoma, MCF-7 breast carcinoma, SW 620 and LoVo colon carcinoma, HCT-116 ilocecal carcinoma, PC-3 prostate carcinoma, MeVo melanoma, and A2780 ovarian carcinoma, as well as two sublines selected for resistance to doxorubicin (A2780/Dx and MCF-7/Dx) and a subline selected for resistance to cisplatin (A2780/DDP). Sensitive tumor cells were obtained from the American Type Culture Collection, whereas resistant tumor cells were from the Istituto Tumori of Milan. All cell lines were grown as monolayers in RPMI-1640 (Life Technologies, Inc., New York) containing 10% fetal bovine serum (Life Technologies, Inc.).

Drug Treatment. Cells were grown in a volume of 100 μL at approximately 10% confluency in 96-well multititer plates and were allowed to attach and recover for another 24 h. Varying concentrations of drugs alone were then added to each well, the plates were incubated in an atmosphere of 5% CO_2 and 95% air at 37 °C for an additional 24 h, and then the plates were washed to remove drug and incubated for 48 h. Control cultures included equivalent amounts of vehicle used to solubilize each molecule. Experimental agent nos. 3−10 were solubilized in DMSO while nos. 11−17 and doxorubicin were dissolved in water.

Sulforhodamine B Assay. At the end of the treatment, cell viability was assessed by the sulforhodamine B (SRB) assay.[34] Data were expressed as T/C (%) = (OD of treated cells/OD of control cells) × 100, and the concentration of the test compound causing a 50% inhibition of cell growth (IC_{50}) was calculated from the dose/effect curve for each tested compound. Every assay was performed in triplicate, and the drug IC_{50} of each cell line was the average of at least three independent experiments.

Human Topoisomerase IIα Relaxation Assay. Purified top2 was purchased from TopoGEN (Columbus, OH). For the assay 0.2 μg of supercoiled pBR322 DNA (Takara Shuzo Co., Ltd., Otsu, Japan) was relaxed by 1 unit of top2 in a total volume of 20 μL of assay buffer in the presence of various concentrations of the drugs for 1 h at 30 °C. At the end of the incubation period the DNA samples were subjected to electrophoresis in a 1% agarose gel with TBE running buffer at a voltage of 1 V/cm for approximately 18 h. After the run the gel was stained with 1 μg/mL ethidium bromide for 30 min followed by destaining in distilled water for 30 min. The DNA topoisomers were photographed under UV light.

Circular Dichroism (CD). All CD spectra were recorded using a JASCO J710 spectropolarimeter, with a cell of 1 mm path length. The CD analyses were performed using a measurement range from

500 to 240 nm, a 2 nm bandwidth, four accumulations, and a 100 nm/min scanning speed at 25 °C.

NMR Spectroscopy. NMR experiments were performed on a Varian Mercury 500 MHz spectrometer at 298 K. NMR samples were prepared by dissolving each compound (about 5 mM) in 0.6 mL of $CDCl_3$ (Sigma-Aldrich). For the absolute stereochemistry determination, compounds **7a** and **7b** were dissolved in DMSO-d_6 (Sigma-Aldrich) since this solvent allowed a better dispersion of the aliphatic proton signals. 2D NOESY[22] spectra were recorded in the phase-sensitive mode, and data block sizes were 2048 addresses in t_2 and 512 equidistant t_1 values. Before Fourier transformation, the time domain data matrices were multiplied by shifted $\sin^2$ functions in both dimensions.

a. STD-NMR. STD-NMR experiments were performed on a Varian Inova 700 MHz spectrometer at 298 K. NMR samples were prepared by dissolving the ligand and the calf thymus DNA (Sigma-Aldrich) or poly(dG-dC)·poly(dG-dC) copolymer (Pharmacia Biochemicals) in D_2O (600 μL, 99.996%, CIL Laboratories) containing phosphate-buffered saline at pH 7.1. A high ligand−receptor molar excess (20:1) was used for the best STD effects. In particular, the concentration of **7a** and **16a** was 1.0 mM, whereas that of the DNA was 50 μM, expressed as the molarity of phosphate groups. The STD effects of the individual protons were calculated for each compound relative to a reference spectrum with off-resonance saturation at $\delta = -16$ ppm. Typically, 64 scans were recorded for the reference STD spectrum, whereas 1024 scans were recorded for each DF−STD spectrum (saturation time 2 s). The relative STD effect was calculated for each signal as the difference between the intensity (expressed as the S/N ratio) of one signal in the on-resonance STD spectrum and that of the same signal in the off-resonance NMR spectrum divided by the intensity of the same signal in the off-resonance spectrum. BMI values were obtained as the ratio of the relative STD effects upon irradiation at 9.0 and 0.5 ppm.[30]

Computational Chemistry. Molecular modeling and graphics manipulations were performed using the InsightII software package (Accelrys, San Diego, CA) running on a Silicon Graphics Octane2 workstation and on a Dell Precision 780, a dual-core Pentium D 3800 GHz machine running Linux RedHat Enterprise WS 4.0 as the operating system.

a. Model Building and Ligand Docking. The NMR structure of the DNA octamer $[d(ACGTACGT)]_2$ complexed with WP631 (PDB entry code 1AL9)[32] was retrieved from the RCSB Protein Data Bank.[35] To obtain the DNA octamer $[d(ACGTACGT)]_2$, used for our docking, the ligand WP631 was removed from the original PDB file. Missing hydrogens and CVFF (consistent-valence force field)[36] partial atomic charges were added using the Biopolymer module of the InsightII program (Accelrys). After assignment of bond orders, missing hydrogen atoms were added and a short minimization (100 steepest descent steps using the CVFF with a gradient convergence value of 0.05 kcal/(mol Å)) was performed using the Discover module present in the InsightII program to release any internal strain. Then in the AutoDockTools package,[31] the partial atomic charges were calculated using the Gasteiger−Marsili method,[37] and after merging of nonpolar hydrogens, rotable bonds were assigned. The 3D structures of compounds **7a** and **7b** were constructed using the module Builder of the InsightII program and then optimized using a molecular dynamics simulation calculation performed by a simulated annealing method,[38] in vacuo, using the CVFF in the InsightII/Discover software packages.

Automated docking studies were carried out using AutoDock version 3.0.5.[31] The grid maps representing the DNA in the actual docking process were calculated with AutoGrid (part of the AutoDock package). The grids (one for each atom type in the ligand, plus one for electrostatic interactions) were chosen to be sufficiently large to include not only the active site but also significant portions of the surrounding surface. The points of the grids were thus 50 × 50 × 50 Å with a grid spacing of 0.375 Å (roughly a quarter of the length of a carbon−carbon single bond), and because the location of the original ligand in the complex was known, the cubic grids were centered on the ligand's binding site.

The grid was centered on the central axis of DNA and particularly between 5′-C2G7-3′ and 5′-G3C6-3′ of double-strain DNA. Of the three different search algorithms offered by AutoDock 3.0.5, the Lamarckian genetic algorithm (LGA) was applied to model the interaction/binding between DNA and compounds **7a** and **7b**. For the local search, the so-called pseudo-Solis and Wets algorithm[39] was used. The docking process was performed in two steps. In the first short step, consisting of 100 LGA runs, the initial position of the ligand was random. The population was 50, the maximum number of generations was 27000, and the maximum number of energy evaluations was limited to 250000. The best ligand orientation in the first step, based on the score criteria, was used as the input position for the second docking step, where the number of energy evaluations was 2.5×10^6. The second step provided the most probable ligand geometries and orientations in the binding pocket. The resultant ligand orientations and conformations were scored on the basis of the docking and binding energies (the cutoff value for the energies was 2 kcal/mol). Multiple docking runs can increase the performance of docking programs,[40] as was shown specifically in the case of AutoDock.[41] To meet aspects of calculation time and data size on one hand and convergence criteria and statistical relevance on the other hand, 50 independent docking runs were performed for each docking case. Cluster analysis was performed on the docked results using a root-mean-square (rms) tolerance of 0.5 Å.

b. Molecular Dynamics Simulations. The best scored complex structure obtained by AutoDock was subjected to molecular dynamics calculations. First, the complex was energy-minimized using the steepest descent algorithm until the maximum rms derivative was less than 0.01 kcal/Å, followed by MD production runs of 70 ps, initiated after the system was heated from 100 to 300 K over 2 ps. During molecular dynamics, frame structures were saved every 1 ps. The average conformation was extracted and again energetically minimized by a combination of steepest descent and a conjugate gradient minimization algorithm until the maximum derivative was less than 0.01 kcal/Å. The Homology InsightII module was used to check some structural properties (bond distances, bond angles, torsion angles, rmsd, hydrogen bonds). The hydrogen bond criterion was a maximum donor−acceptor distance of 3.5 Å and a minimum donor−proton−acceptor angle of 120°.

Acknowledgment. The LC−MS and NMR spectral data were provided by Centro di Ricerca Interdipartimentale di Analisi Strumentale, Università degli Studi di Napoli "Federico II". The assistance of the staff is gratefully appreciated.

Supporting Information Available: Microanalytical, ^{13}C NMR, and CD data for all test compounds and 2D NOESY spectra for compounds **7a**, **7b**, **8a**, **8b**, **9a**, **9b**, **14a**, and **14b**. This material is available free of charge via the Internet at http://pubs.acs.org.

References

(1) De Vita, V. T.; Hellman, S.; Rosenberg, S. A. *Cancer: Principles and Practice of Oncology*, 6th ed.; Lippincott, Williams and Wilkins: Philadelphia, PA, 2001.
(2) Lown, J. W. Anthracycline and Anthraquinone Anticancer Agents: Current Status and Recent Developments. *Pharmacol. Ther.* **1993**, *60*, 185−214.
(3) Serrano, J.; Palmeira, C. M.; Kuehl, D. W.; Wallace, K. B. Cardioselective and Cumulative Oxidation of Mitochondrial DNA Following Subchronic Doxorubicin Administration. *Biochim. Biophys. Acta* **1999**, *1411*, 201−205.
(4) Endicott, J. A.; Ling, V. The Biochemistry of P-Glycoprotein-Mediated Multidrug Resistance. *Annu. Rev. Biochem.* **1989**, *58*, 137−171.
(5) Baird, R. D.; Kaye, S. B. Drug Resistance Reversal-Are We Getting Closer? *Eur. J. Cancer* **2003**, *39*, 2450−2461.
(6) Thigpen, J. T. Innovations in Anthracycline Therapy: Overview. *Community Oncol.* **2005**, *2* (S1), 3−7.
(7) Binaschi, M.; Bigioni, M.; Cipolline, A; Rossi, C.; Goso, C.; Maggi, C. A.; Capranico, G.; Animati, F. Anthracyclines: Selected New Developments. *Curr. Med. Chem.: Anti-Cancer Agents* **2001**, *1*, 113−130.

(8) Pezzoni, G.; Beggiolin, G.; Manzotti, C.; Spinelli, S.; Tornella, S.; Giuliani. F. C. BBR 2778, a Novel Aza-Analogue of Anthracenediones Endowed with Preclinical Anticancer Activity. *Proc. Am. Assoc. Cancer Res.* **1993**, *34*, Abstract 2226.
(9) Gogas, H.; Mansi, J. L. The Anthrapyrazole. *Cancer Treat. Rev.* **1995**, *21*, 541−552.
(10) Krapcho, A. P.; Menta, E.; Oliva, A.; Di Domenico, R.; Fiocchi, L.; Maresch, M. E.; Gallagher, C. E.; Hacker, M. P.; Beggiolin, G.; Giuliani, F. C.; Pezzoni, G.; Spinelli, S. Synthesis and Antitumor Evaluation of 2,5-Disubstituted-Indazolo[4,3-*gh*]isoquinolin-6(*2H*)-ones (9-Aza-anthrapyrazoles). *J. Med. Chem.* **1998**, *41*, 5429−5444.
(11) Collier, D. A.; Neidle, S. Synthesis, Molecular Modelling, DNA Binding, and Antitumor Properties of Some Substituted Amidoanthraquinones. *J. Med. Chem.* **1988**, *31*, 847−857.
(12) Gatto, B.; Zagotto, G.; Sissi, C.; Cera, C.; Uriarte, E.; Palù, G.; Capranico, G.; Palumbo, M. Peptidyl Anthraquinones as Potential Antineoplastic Drugs: Synthesis, DNA Binding, Redox Cycling, and Biological Activity. *J. Med. Chem.* **1996**, *39*, 3114−3122.
(13) Gerwirtz, D. A. A Critical Evaluation of the Mechanisms of Action Proposed for the Antitumor Effects of the Antrhracycline Antibiotics Adriamycin and Daunorubicin. *Biochem. Pharmacol*. **1999**, *57*, 727−741.
(14) Tewey, K. M.; Chen, G. L.; Nelson, E. M.; Liu, L. F. Intercalative Antitumor Drugs Interfere with the Breakage-Reunion Reaction of Mammalian DNA Topoisomerase II. *J. Biol. Chem.* **1984**, *259*, 9182−9187.
(15) Moro, S.; Beretta, G. L.; Dal Ben, D.; Nitiss, J.; Palombo, M.; Caprinico, G. Interaction Model for Anthracycline Activity against DNA Topoisomerase II. *Biochemistry* **2004**, *43*, 7503- 7510.
(16) Cummings, J.; Mincher, D. J.; Maepherson, J. L. Rational Design of Anthracenyl-Peptide Topoisomerase II Inhibitions. *Ann. Oncol.* **1992**, *3*, (Suppl. 1), Abstract 128.
(17) Wang, J. C. DNA Topoisomerases. *Annu. Rev. Biochem*. **1996**, *65*, 635−692.
(18) Gomez-Monterrey, I.; Campiglia, P; Mazzoni, O.; Novellino, E.; Diurno, M. V. Cycloaddition Reactions of Thiazolidine Derivatives. An Approach to the Synthesis of New Functionalized Heterocyclic Systems. *Tetrahedron Lett.* **2001**, *42*, 5755−5757.
(19) Gomez-Monterrey, I.; Campiglia, P; Grieco, P.; Diurno, V. M.; Bolognese, A.; La Colla, P.; Novellino, E. New Benzo[*g*]isoquinoline-5,10-diones and Dihydrothieno[2,3-*b*]naptho-4,9-dione Derivatives: Synthesis and Biological Evaluation as Potential Antitumoral Agents. *Bioorg. Med. Chem.* **2003**, *11*, 3769−3775.
(20) Gomez-Monterrey, I.; Santelli, G.; Campiglia, P.; Califano, D.; Falasconi, F.; Pisano, C.; Vesci, L.; Lama, T.; Grieco, P.; Novellino, E. Cytotoxic Evaluation of Novel Spirohydantoin Derivatives of the Dihydrothieno[2,3-*b*]naphtho-4,9-dione System. *J. Med. Chem.* **2005**, *48*, 1152−1157.
(21) Rittle, K. E.; Evans, B. E.; Bock, M. G.; Di Pardo, R. M.; Whitter, W. L.; Homnick, C. F.; Veber, D. F.; Freidinger, R. M. A New Amine Resolution Method and Its Application to 3-Amino Benzodiazepines. *Tetrahedron Lett.* **1987**, *28*, 521−522.
(22) Jenner, J.; Meyer, B. H.; Bachman, P.; Ernst, R. R. Investigation of Exchange Processes by Two-Dimensional NMR Spectroscopy. *J. Chem. Phys.* **1979**, *71*, 4546−4553.
(23) Eliel, E. L.; Wilen, S. H. *Stereochemistry of Organic Compounds*; John Wiley & Sons, Inc.: New York, 1994; pp 1113−1119.
(24) Pommier, Y.; Fesen, M. R.; Goldwasser, F. Topoisomerase II Inhibitors: the Epipodophyllotoxins, *m*-AMSA, and the Ellipticine Derivatives. *Cancer Chemotherapy and Biotherapy: Principles and Practice*; Lippincott-Raven: Philadelphia, 1996; pp 435−461.
(25) Su, T-L.; Chou, T-C.; Kim, J. Y.; Huang, J-T.; Ciszewska, G.; Ren, W-Y.; Otter, G. M.; Sirotnak, F. M.; Watanabe, K. A. 9-Substituted Acridine Derivatives with Long Half-Life and Potent Antitumor Activity: Synthesis and Structure-Activity Relationships. *J. Med. Chem.* **1995**, *38*, 3226−3235.
(26) Wang, L.; Price, H. L.; Juusola, J.; Kline, M.; Phanstiel IV, O. Influence of Polyamine Architecture on the Transport and Topoisomerase II Inhibitory Properties of Polyamine DNA-Intercalator Conjugates. *J. Med. Chem.* **2001**, *44*, 3682−3691.
(27) Nagarajan, M.; Morrell, A.; Fort, B. C.; Meckley, M. R.; Antony, S.; Kohlhagen, G.; Pommier, Y.; Cushman, M. Synthesis and Anticancer Activity of Simplified Indenoisoquinoline Topoisomerase I Inhibitors Lacking Substituents on the Aromatic Ring. *J. Med. Chem.* **2004**, *47*, 5651−5661.
(28) Mayer, M.; Meyer, B. Characterization of Ligand Binding by Saturation Transfer Difference NMR Spectroscopy. *Angew. Chem., Int. Ed.* **1999**, *38*, 1784−1788.
(29) Meyer, B.; Peters, T. NMR Spectroscopy Techniques for Screening and Identifying Ligand Binding to Protein Receptors. *Angew. Chem., Int. Ed.* **2003**, *42*, 864−890.
(30) Di Micco, S.; Bassarello, C.; Bifulco, G.; Riccio, R.; Gomez-Paloma, L. Differential-Frequency Saturation Transfer Difference NMR Spectroscopy Allows the Detection of Different Ligand−DNA Binding Modes. *Angew. Chem., Int. Ed.* **2006**, *45*, 224−228.
(31) (a) Goodsell, D. S.; Olson, A. J.; Automated Docking of Substrates to Proteins by Simulated Annealing. *Proteins: Struct., Funct., Genet.* **1990**, *8*, 195−202. (b) Morris, G. M.; Goodsell, D. S.; Huey, R.; Olson, A. J.; Distributed Automated Docking of Flexible Ligands to Proteins: Parallel Applications of AutoDock 2.4. *J. Comput.-Aided Mol. Des.* **1996**, *10*, 293−304. (c) Morris, G. M.; Goodsell, D. S.; Halliday, R. S.; Huey, R.; Hart, W. E.; Belew, R. K.; Olson, A. J. Automated Docking Using Lamarckian Genetic Algorithm and an Empirical Binding Free Energy Function. *J. Comput. Chem.* **1998**, *19*, 1639−1662.
(32) Robinson, H.; Priebe, W.; Chaires, J. B.; Wang, A. H. Binding of Two Novel Bisdaunorubicins to DNA Studied by NMR Spectroscopy. *Biochemistry* **1997**, *36*, 8663−8670.
(33) Brooks, B. R.; Bruccoleri, R. E.; Olafson, B. D.; States, D. J.; Swaminathan, S.; Karplus, M. CHARMM: A Program for Macromolecular Energy, Minimization and Dynamics Calculations. *J. Comput. Chem.* **1983**, *4*, 187−217.
(34) Skehan, P.; Storeng, R.; Scudiero, D.; Monks, A.; McMahon, J.; Vistica, D.; Warren, J. T.; Bokesch, H.; Kenney, S.; Boyd, M. R. New Colorimetric Cytotoxicity Assay for Anticancer-Drug Screening. *J. Natl. Cancer Inst.* **1990**, *82*, 1107−1112.
(35) Bernstein, F. C.; Koetzle, T. F.; Williams, G. J. B.; Meyer, E. F., Jr.; Brice, M. D.; Rodgers, J. R.; Kennard, O.; Shimanouchi, T.; Tasumi, T. The Protein Data Bank: A Computer Based Archival File for Macromolecular Structures. *J. Mol. Biol.* **1977**, *112*, 535−542.
(36) Maple, J.; Dinur, U.; Hagler, A. T. Derivation of Force Fields for Molecular Mechanics and Dynamics from ab Initio Energy Surface. *Proc. Natl. Acad. Sci. U.S.A.* **1988**, *85*, 5350−5354.
(37) Gasteiger, J.; Marsili, M. Iterative Partial Equalization of Orbital Electronegativity−a Rapid Access to Atomic Charges. *Tetrahedron* **1980**, *36*, 3219−3228.
(38) Nilges, M.; Clore, G. M.; Gronenborn, A. M. Determination of Three-Dimensional Structures of Proteins from Interproton Distance Data by Dynamical Simulated Annealing from a Random Array of Atoms. Circumventing Problems Associated with Folding. *FEBS Lett.* **1988**, *239*, 129−136.
(39) Solis, F. J.; Wets, R. J. B. Minimization by Random Search Techniques. *Math. Oper. Res.* **1981**, *6*, 19−30.
(40) McConkey, B. J.; Sobolev, V.; Edelman, M. The Performance of Current Methods in Ligand-Protein Docking. *Curr. Sci.* **2002**, *83*, 845−856.
(41) Wang, R. X.; Lu, Y. P.; Wang, S. M. Comparative Evaluation of 11 Scoring Functions for Molecular Docking. *J. Med. Chem.* **2003**, *46*, 2287−2303.

JM0612158